LNGS - 95/10
May 1995

A FIRST 600 TON ICARUS DETECTOR INSTALLED AT THE GRAN SASSO LABORATORY

ADDENDUM

to proposal LNGS – 94/99 I&II

by the ICARUS Collaboration

19 May 1995

P. Cennini, S. Cittolin, G.Maurin, A. Placci, J.P. Revol, C. Rubbia*, W.H. Tian

CERN, CH-1211 Geneva 23, Switzerland

J.M. Ma, L.K. Ding, Y. Li, F. Lu, J.F. Qiu, H.Y. Sheng, K.L Tung, J.Y. Zeng, B. Zhang

Institute of High Energy Physics, Beijing, People's Republic of China

F. Casagrande, D. Dzialo Giudice, X. Li, G. Mannocchi, S. Motto, P. Picchi

Lab. Naz. di Frascati dell'INFN, via E. Fermi 40, Frascati (Roma), Italy

P. Boccaccio

Lab. Naz. di Legnaro dell'INFN, via Romea 4, Legnaro (PD) , Italy

F. Cavanna, E. Olejarczyk, G. Piano Mortari, M. Verdecchia

Dipartimento di Fisica e INFN, Università dell'Aquila, via Vetoio, L'Aquila, Italy

D. Cline, W. Hong, G. Muratori, S. Otwinowski, J. Park, H.G. Wang, M. Zhou

Department of Physics, UCLA, Los Angeles, CA 90024, USA

A. Bettini, S. Centro, C. De Vecchi, A. Pepato, F. Pietropaolo, S. Ventura

Dipartimento di Fisica e INFN, Università di Padova, via Marzolo 8, Padova, Italy

P. Benetti, E. Calligarich, S. Cesana, R. Dolfini, A. Gigli Berzolari, F. Mauri, L. Mazzone, C. Montanari, A. Piazzoli, A. Rappoldi, G.L. Raselli, M. Rosella, D. Scannicchio, M. Terrani, C. Vignoli

Dipartimento di Fisica e INFN, Università di Pavia, via Bassi 6, Pavia, Italy

F. Sergiampietri

INFN Pisa, via Livornese 1291, 56010 S. Piero a Grado, Pisa, Italy

L. Periale, S. Suzuki

ICGF del CNR di Torino, corso Fiume 4, Torino, Italy

E. Fenyves

University of Texas at Dallas, Dallas, Texas, USA

* Spokesman of the Collaboration.

CONTENTS

I. INTRODUCTION

The ICARUS physics programme described in Volume I of our proposal [1] has been endorsed by the entire physics community, since, not only Europe, but also America and Japan are now setting up programmes with similar goals. Therefore it has become very important to make sure that the final phase of the ICARUS project requiring a sensitive mass of liquid argon of 5000 tons or larger, be achieved in the most time efficient way. It appears to us that the best way to reach the sensitive mass needed to fulfil our scientific goals is to go through an intermediate step between the 3 ton detector [2] in operation at CERN and the major engineering design described in Volume II of our proposal [1]. A few hundred ton detector will insure that our extrapolation between 3 tons and a few thousand tons is done in the most efficient way.

This step-wise strategy will allow us to develop progressively, at the Gran Sasso Laboratory, (1) the infrastructure needed to build and operate our large detector, (2) the *in situ* experience needed in terms of safety but on a still modest liquid argon volume, and (3) to obtain a definitive and practical evaluation of our engineering choice for the final phase.

It quickly appeared to us, that a few hundred ton detector would at the same time allow an important first step in our scientific programme. What the bubble chamber like ICARUS technique is providing, is a background-free detection of proton decay and neutrino events. While a sensitive mass in excess of a few thousand tons of liquid argon is clearly needed to achieve the 10^{34} years range in proton decay lifetime in a number of proton decay channels, many exotic channels have only been poorly investigated so far or not at all, and would be easily covered in this first phase. Atmospheric and solar neutrinos are areas which could be completely clarified in establishing whether the effects observed by Kamiokande [3] and Homestakes [4] are instrumental or genuine. Therefore we have chosen a detector size which is the largest which can be transported from an outside laboratory to the Gran Sasso Laboratory: two half detectors with a cross-section of 3.9 by 4.2 metres and a length of 19 metres, corresponding to a total internal volume of 465 m^3 and a sensitive mass of 540 tons of liquid argon. Moreover we decided to use a 3 mm wire pitch instead of the 5 mm foreseen for the 5000 ton module, in order to allow for higher precision measurements. This is particularly beneficial for solar neutrinos, especially when this is combined also with the presence of a neutron absorber around the entire volume, in order to reduce the radioactivity background to a negligible level.

This choice is ideal to fulfil the two goals discussed above: an intermediate technical step between 3 tons and 5000 tons and a first important part of the ICARUS physics programme within a time scale of two years. This intermediate step opens in addition the possibility to explore a new route towards larger detector volumes: the construction of a number of identical 600 ton detectors installed next to one another.

II. PHYSICS WITH A 600 TON DETECTOR

We will not repeat here what was already stated clearly in Volume I of our proposal, but we can stress again our general scientific strategy before we review specifically which physics programme we can envisage with a sensitive mass of 540 tons.

The necessity of going beyond the Standard Model is inescapable. Some of the most fundamental physics issues are involved: (1) Gran Unification; (2) CP and/or CPT violation; (3) new symmetries (SUSY, etc.); (4) cosmology, etc. LHC is the main new enterprise in HEP, however, its indent on the Standard Model is necessarily limited by the constituent energy ≤ 1 TeV. The answer to many fundamental questions lies beyond the experimental possibility of particle colliders: (1) matter stability (GUTs, etc.); (2) neutrino masses and mixing (right-handed leptons, See-Saw mechanism, etc.).

A different experimental methodology must be introduced: propagator physics must replace direct observations. This method has already proven to be very effective. For instance, almost all properties of the W and Z weak bosons were already known from β-decay, also, neutral currents and photo-production are studied at HERA without real photons.

Studying the stability of matter may be the most important challenge facing present time Particle Physics. The experimental challenge matches the importance of the issue because of the very high energy scale involved and the progress needed in the detector technology.

We believe that ICARUS represents the ideal detector for rare event search, such as proton decays and neutrino interactions. Traditional bubble chambers have played a fundamental role in Particle Physics because they provide non-biased images, in three dimensions and with high resolution. The ICARUS Collaboration has developed a new generation of bubble chambers, operated over a very large sensitive volume, continuously sensitive, self-triggering, able to provide three-dimensional views of ionising events with particle identification from dE/dx and range measurements.

With ICARUS we are entering a second generation phase for neutrino and proton decay physics. Our first 600 ton module has a mass close to the Kamiokande detector mass, but the higher efficiency and the much more detailed information which can be collected for each event should rapidly allow us to reach definite conclusions on the phenomena to be studied. A brief description of the physics programme which can be achieved with the first 600 ton detector at Gran Sasso is given below.

A clear difference with the programme we proposed with 5000 ton modules, is the fact that we can put more emphasis on solar neutrinos, because the smaller size of the detector allows for higher resolution, lower background (external shielding) and the unique possibility to measure for the first time the ^{8}B neutrino energy spectrum, using neutrino scattering on deuterium. We can indeed dope the liquid argon with deuteriated methane

(CD_4). The quasi free deuterium atoms allow a rather simple kinematics of the scattering process, and the resulting outgoing electron spectrum reflects closely the initial solar neutrino (ν_e) spectrum. If the solar neutrino problem is real, and if the MSW effect is at work, a distortion of the Standard Solar Model ^8B neutrino spectrum will be observed by ICARUS.

This study was not envisaged for our 5000 ton module, but the smaller size of the technical module under consideration here, allows us to consider this possibility which we had already proposed in our initial proposal [10].

This measurement of the shape of the solar ^8B neutrino spectrum should provide the first direct test, independent of solar models, of the oscillation hypothesis, as a possible solution to the present apparent puzzle. With the 600 ton ICARUS intermediate module, solar neutrinos become one of the main short term priorities.

Finally, the 600 ton ICARUS module, which should be operational in about two years, will be ready to receive neutrinos from CERN, should the CERN neutrino beam to Gran Sasso be approved promptly. The expected sensitivity covers the areas indicated by Kamiokande atmospheric neutrino data, and will allow to distinguish between the type of neutrino oscillations which may be observed.

1. Atmospheric neutrinos

1.1 The atmospheric neutrino puzzle: an update

The atmospheric neutrino issue is currently considered one of the most burning and debated questions in HEP. Amongst various studies performed by different experiments, the Kamiokande results are presently the most significant.

Initially, the Kamiokande group separated muons from electrons in the observed low energy, contained neutrino event sample (the so-called "sub-GeV" sample). It was found that the ratio of muon to electron events was smaller than expected $[(\mu/e)_{data}/(\mu/e)_{MC} = 0.60)]$ [3]. This result was interpreted as a possible hint for neutrino flavour oscillations, assuming that the smallness of the ratio is due to a depletion of the muon neutrino event sample.

A recent study by Kamiokande of the neutrino data in the so-called "multi-GeV" energy range provided a new measurement from an independent data sample, of the μ-like to e-like event ratio $[(\mu/e)_{data}/(\mu/e)_{MC}) = 0.57]$ [5]. In addition, the better angular correlation between the neutrinos and the produced charged-leptons for these "multi-GeV" events provided valuable information on neutrino oscillations, by studying the zenith-angle dependence of the (μ/e) ratio.

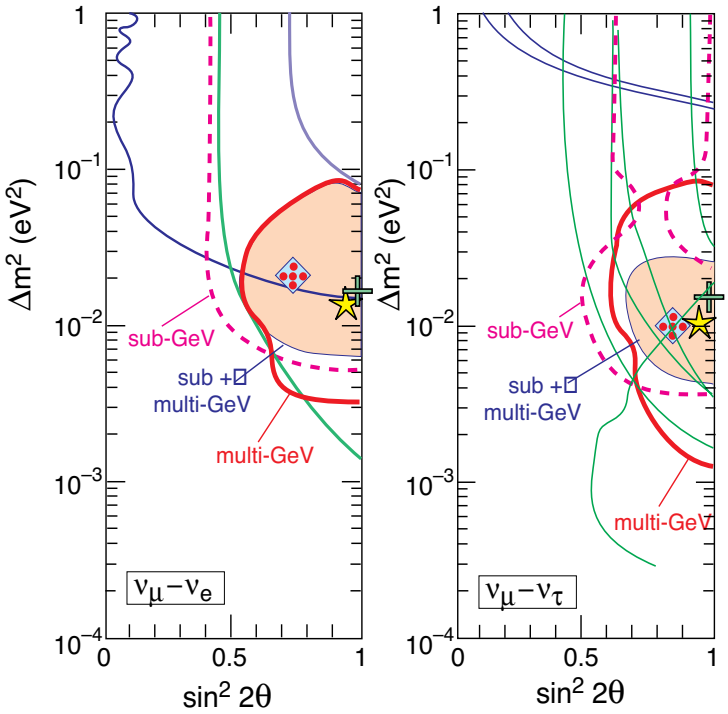

Figure 1.1: Summary of Kamiokande atmospheric neutrino data [5]. 90% C.L. allowed neutrino oscillation parameters as obtained from the "Multi-GeV data (thick curves). 90% C.L. allowed regions as obtained from the updated "Sub-GeV" data are also shown (Thick dotted curves). The combined allowed regions are shown as grey areas.

Therefore, the overall analysis of the Kamiokande data strengthened the neutrino oscillation hypothesis and yielded allowed regions of the oscillation parameters for both the ($\nu_\mu \leftrightarrow \nu_e$) and ($\nu_\mu \leftrightarrow \nu_\tau$) channels (Figure 1.1).

On the other hand, a recent study [6] on a possible underestimated neutron background from muon interactions in the surrounding rocks showed that the electron sample from Kamiokande and IMB experiments could be contaminated by π^0's from isolated neutrons faking the electron signature, ($n + Ar \rightarrow \pi^0 + X$). Taking into account this extra background, the authors of Ref. [6] concluded that the atmospheric neutrino anomaly vanishes completely.

A new experiment (Super-Kamiokande), using the same water-Cerenkov technique as Kamiokande will be ready by the end of 1996 and is expected to provide further data on this issue, with reduced statistical error. However, a new generation experiment characterised by a better e/μdiscrimination, by a clear discrimination between electrons and π^0's to reduce the neutron background, by a higher precision on energy and direction measurements and by a better reconstruction efficiency seems to be necessary to definitely clarify the atmospheric neutrino issue.

The "600 ton-ICARUS" experiment at the Gran Sasso laboratory (under a thick rock cover of 4200 metres of water equivalent) is ideally suited to perform the atmospheric neutrino study in a short time scale and with sufficient sensitivity to cover the present Kamiokande allowed regions in the neutrino oscillation parameter space.

1.2 Atmospheric neutrino interaction rate in the 600 ton ICARUS detector

The calculation of the neutrino-induced event rate expected in case of no oscillation, is based on the convolution of the flux with the cross-section for neutrino interaction, in a detector with a given detection efficiency and acceptance. To calculate this rate in the 600 ton-ICARUS detector we used the same set of cosmic fluxes from the Bartol Group [7], used in the Proposal for the 5-kton experiment (Vol. 1, section 2.3.1) and the interaction cross-sections on liquid argon have been calculated with the GENEVE Monte Carlo generator [8]. A new version of the GENEVE code includes also the set of neutral-current cross-sections. At this stage we assume a full detection efficiency and we calculate the charged and neutral currents event rates (without oscillations) in one year, for a sensitive mass of 540 tons, which means that we count the number of events with a vertex within this sensitive mass, regardless of whether the outgoing particles are contained or not.

With these assumptions, we give the expected number of events for the various neutrino species, integrating over two different solid angle regions of $\Delta\Omega = 2\pi$, corresponding to the top and bottom hemispheres seen by the detector. The following predictions use $M_A = 1.03$ GeV [9] (mass in the axial vector form factor), and the systematic error on M_A is estimated to be of the order of 15%.

Charged current events. The number of events are computed for ν_e energies larger than 50 MeV while for ν_μ's it is all events above the threshold of 130 MeV:

	ν_μ	$\bar{\nu}_\mu$	ν_e	$\bar{\nu}_e$	**Total**
Top	33	12	24	7	77
Bottom	29	11	21	7	67
				Overall	**144**

Neutral current events (only quasi-elastic reaction: $p + \nu \rightarrow p + \nu$). This process produces heavily ionising tracks, on average 5 cm long. For neutral current events, all the rates are for neutrino energies above 50 MeV:

	ν_μ	$\bar{\nu}_\mu$	ν_e	$\bar{\nu}_e$	**Total**
Top	5	2	2.5	1.5	11
Bottom	4	2	2	1	8.5
				Overall	**20**

To these 20 quasi-elastic events on protons, one can add 40.5 quasi-elastic events on neutrons. In both cases a Monte Carlo study is still needed to find out how well N.C. events can be reconstructed. In principle the combined information from C.C. and N.C. events can help distinguish $\nu_\mu \leftrightarrow \nu_e$ from $\nu_\mu \leftrightarrow \nu_\tau$ oscillations, independently of the magnitude of the primary cosmic neutrino flux, however, this method requires large statistics.

1.3 Containment of Atmospheric Neutrinos

Atmospheric neutrino interactions produce low multiplicity events with a lepton (μ or e) accompanied by a nucleon (p or n) and eventually by one (or two) pion(s). The event occupancy in the liquid argon sensitive volume depends on the neutrino energy and on the final state signature. A fiducial volume ensuring the full event containment, inside the sensitive volume, has to be defined on statistical basis from MC simulation.

In this preliminary study we have simply defined a common geometrical acceptance for both muon and electron events. Since muons have the longest *mean range* [1] (about 1.3 m at a kinetic energy of 300 MeV), the acceptance is defined from the requirement that atmospheric neutrino events containing a muon in final state are contained in the detector.

Therefore we studied the percentage of muon events totally contained in the 540 ton ICARUS sensitive volume as a function of the incident neutrino energy (Figure 1.2). This distribution was obtained generating ν_μ C.C. interactions at fixed neutrino energies with vertices uniformly

[1]We define as *mean range* the average radius of the smallest spherical volume which contains all the charged tracks in the event. This was simulated with the help of the GEANT code.

distributed in the sensitive volume. Convoluting the result with the event distribution expressed also as a function of the incident neutrino energy, we obtained an overall acceptance $\alpha_\mu = 72\ \%$ to be applied to the sensitive volume of 540 tons.

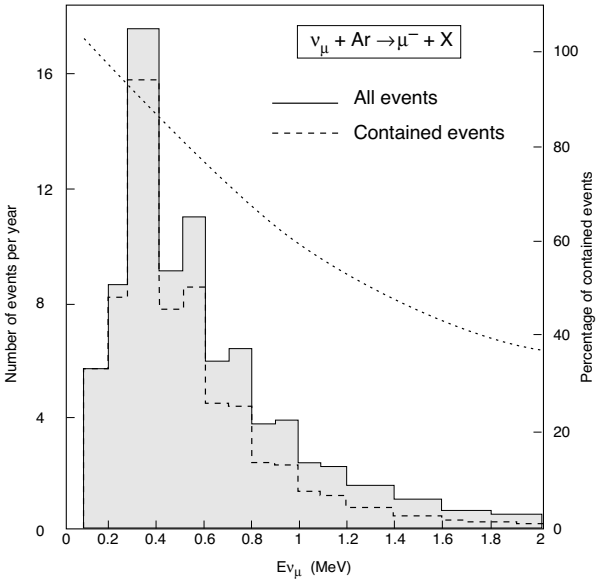

Figure 1.2: The dotted line shows the percentage of contained ν_μ C.C. events (right-hand scale) as a function of the incident ν_μ energy. The grey histogram shows the number of ν_μ C.C. interactions in the detector sensitive volume and the dashed histogram shows the fraction of those events contained in the sensitive volume, as a function of the incident ν_μ energy.

For the oscillation sensitivity study, we used the fully contained events data sample.

1.4 Sensitivity to oscillations with atmospheric ν's data

We performed separately the study of the sensitivity to oscillations in the ($\nu_\mu \leftrightarrow \nu_\tau$) sector and in the ($\nu_\mu \leftrightarrow \nu_e$) sector where upward-going neutrinos undergo matter effects while crossing the Earth matter.

1.4.1 The ($\nu_\mu \leftrightarrow \nu_e$) case

The oscillation study with the 5-kton ICARUS detector showed a high sensitivity to ($\nu_\mu \leftrightarrow \nu_e$) oscillations ($\sin^2(2\theta) < 10^{-2}$ for small Δm^2 values between 10^{-4} to 10^{-3} eV^2) mainly due to the MSW enhanced transition probability of the upward-going neutrino sample.

With the 600 ton-ICARUS detector the available statistics are reduced and consequently the sensitivity at small Δm^2 values is strongly weakened by the increased statistical error. A better sensitivity in $\sin^2(2\theta)$ is expected at higher Δm^2 values (10^{-1} to 1 eV^2) corresponding to short range oscillations (few tens of km) where downward-going atmospheric neutrinos can contribute significantly. Therefore, we considered the sensitivity to oscillations from both upward-going (taking into account matter effects across the Earth) and downward-going neutrinos crossing the Earth's

atmosphere (vacuum oscillations). The overall sensitivity at 90% C.L. is obtained by combining the two sensitivity regions:

(1) Upward-going neutrinos may undergo oscillations enhanced by matter effects (MSW), depending on the path length and energy (E_ν). The calculation of the neutrino transition probability was performed following the same method reported on the Proposal [1] (Vol. I, section 2.4.1), namely we considered the double ratio R defined as:

$$R = \frac{\rho^{obs}}{\rho^{\exp}}$$

where ρ^{exp} is the ratio of the total number of (ν_μ + **Error!**)$_\mu$) to (ν_e + **Error!**)$_e$) charged current events (from neutrinos with energy larger than 200 MeV) expected in the case of no oscillations, integrating over both energy and zenith angle (limited to the bottom hemisphere).

The ρ^{obs} variable refers to the same quantity, observable in the detector. It depends on the MSW transition probability for both neutrino and antineutrino: matter effects enhance oscillations in the neutrino sector and suppresses slightly oscillations in the anti-neutrino sector, compared to the propagation in vacuum (assuming the standard neutrino mass hierarchy).

The accessible region, in the (Δm^2, $\sin^2 2\theta$) plane is limited by the error (σ_R) on the double ratio R. In this case, the main contribution to σ_R is the statistical error. The systematic error comes from theoretical uncertainties on fluxes and cross-sections, from the acceptance uncertainty and from energy and angular resolution of the ICARUS detector.

For 1 year of running (i.e. an exposure of $\approx$ **0.5** $kton \times yr$) the statistical error is $(\sigma_R/R)_{stat} \approx 25\%$. For an exposure of **1** $kton \times yr$, corresponding to about two to three years of running with the 600 ton ICARUS module, our estimation of the total error is $\sigma_R/R \approx 20\%$, where the statistical contribution is $(\sigma_R/R)_{stat} \approx 19.5\%$. All the other sources of errors contribute to the systematic uncertainty, $(\sigma_R/R)_{syst} \approx 5\%$. We are therefore in a regime where precision is limited by the statistics.

(2) Downward-going neutrinos may undergo oscillations while crossing an average distance of about 15 km, between the production point in the atmosphere and the detector location. The oscillation sensitivity is expressed by the same double ratio R previously defined. However, in this case ρ^{obs} depends on the transition probability calculated in vacuum, since most of the neutrino path is in the atmosphere.

The statistical error on R is approximately the same as that estimated for the up-going neutrinos. For an exposure of **0.5** $kton \times yr$ we have $(\sigma_R/R)_{stat} \approx 27.5\%$. For an exposure of **1** $kton \times yr$ we have $(\sigma_R/R)_{stat} \approx 18.5\%$. In fact, the atmospheric neutrino flux from the top hemisphere is only slightly larger than that from the bottom hemisphere.

The overall sensitivity at 90% C.L. is obtained by combining the two independent sensitivity regions corresponding to up-going and down-going atmospheric neutrinos. In Figure 1.3a two exclusion plots are shown, corresponding to the two exposures considered above (i.e. 1 $kton \times yr$ and 0.5 $kton \times yr$).

We note that the Kamiokande allowed region for $(\nu_\mu \leftrightarrow \nu_e)$ transitions can be covered completely with only one year of exposure time with the 600 ton-ICARUS module.

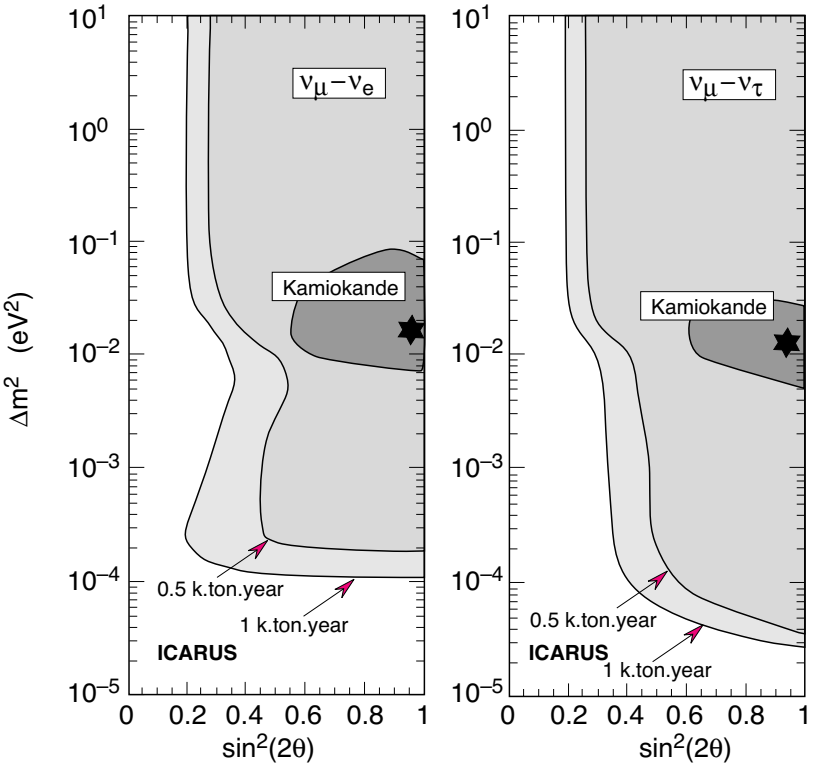

Figure 1.3: 90% confidence level sensitivity regions (on the right hand-side of curves) for the ICARUS 600 ton module separately for (a) $\nu_\mu \leftrightarrow \nu_e$ and (b) $\nu_\mu \leftrightarrow \nu_\tau$ oscillations. Exposure times of 0.5 and 1 k.ton.years are shown.

1.4.2 The ($\nu_\mu \leftrightarrow \nu_\tau$) case

In the $(\nu_\mu \leftrightarrow \nu_\tau)$ case, matter effects do not contribute and ν_μ's may undergo transitions to ν_τ flavour only through vacuum oscillation.

As for the $\nu_\mu \leftrightarrow \nu_e$ case we considered the usual double ratio R, however, in this case the observed number of muons from ν_μ interactions could vary with respect to the expected number, due to ν_μ oscillating to ν_τ, while the number of electrons from ν_e interactions should not change. We assume that $\nu_e \leftrightarrow \nu_\tau$ oscillations are negligible.

The statistical (and total) errors on R for up-going and down-going atmospheric neutrinos are the same as reported in the previous section. The overall sensitivity to $(\nu_\mu \leftrightarrow \nu_\tau)$, at 90% C.L. is obtained by combining the two independent sensitivity regions. In Figure 1.3b two exclusion plots are shown,

corresponding to the two exposures considered above (i.e. 1 $kton \times yr$ and 0.5 $kton \times yr$).

Also in this case, one year of exposure of the 600 ton-ICARUS module to the atmospheric neutrino flux is sufficient to explore the oscillation parameter region indicated by Kamiokande for ($\nu_\mu \leftrightarrow \nu_\tau$) oscillations.

1.5 Conclusion

The preliminary analysis reported here, of the 600 ton-ICARUS sensitivity to oscillation in either sectors ($\nu_\mu \leftrightarrow \nu_e$) or ($\nu_\mu \leftrightarrow \nu_\tau$) confirms that this technical module can provide in a short exposure time (of the order of one year) a conclusive answer to the atmospheric neutrino puzzle reported by the Kamiokande and IMB experiments. The size of this ICARUS module is comparable to the size of Kamiokande but the detector performance and the background level are substantially better.

2. Solar neutrinos

2.1 Solar neutrino scattering on electrons and absorption on Argon

The ICARUS goal in the solar neutrino area is not only to confront the Standard Solar Model, but also to provide a Solar Model independent measurement, by observing several independent processes, as envisaged in our initial proposal [1]:

(1) $\nu_x + e^- \rightarrow \nu_x + e^-$ which occurs with all types of neutrino flavours and for both charged and neutral current exchange.

(2) $\nu_e + Ar \rightarrow K^* + e^-$ which only occurs with the electron neutrino.

The measurement of the ratio of rates for these two processes provides directly a measurement of the ν_e oscillation probability [1].

2.1.1 Data selection

The analysis for the first two reactions has already been widely discussed in our proposal [1], we only recall here what the signatures for these processes are in our detector:

1) $\nu_x + e^- \rightarrow \nu_x + e^-$: one electron with energy larger than 5 MeV, within 25° from the sun direction. The efficiency of this selection is 65%[2]. Because 6% of these events fall under the selection for the absorption channels, the overall efficiency is 61 %. The angular and isolation cuts reduce the background by a factor 20, and the resulting signal is about 290 events per year (Table 2.1), in a fiducial mass of 540 tons.

(2) $\nu_e + Ar \rightarrow K^* + e^-$: this reaction is expected to proceed through two main channels : (a) superallowed Fermi transition to the 4.38 MeV excited isobaric analogue K* state; (b) Gamow-Teller transition to the excited levels below the 4.38 MeV K* state. The two processes are distinguished by the energy and multiplicity of γ ray emitted in the de-excitation of the K* states and by the energy spectrum of the primary electron.

For Fermi events, we require the presence of a 5 MeV electron (this threshold could be chosen at a lower value, since direction measurement in this case is not required), in association with a total energy deposited in a sphere of 50 cm radius around the vertex, larger than 2 MeV. In addition we require that the multiplicity of these Compton electrons of energy larger than 300 keV, be ≥ 3. The resulting efficiency is 76% for Fermi events, and 330 events are expected per year (Table 2.1), in a fiducial mass of 540 tons. There exists a contamination from Gamow-Teller transitions (9% of the Gamow-

[2] In our proposal the selection of elastic scattering events was made using the projection of the angle between the electron reconstructed direction and the sun direction. Here we are using the angle in space. Due to the increased detector resolution, the efficiency happens to be the same in the two cases.

Teller events) and from the elastic channel (less than 1% of the elastic channel events).

For Gamow-Teller events, we have a similar selection as for the Fermi events, except that now we select events with a total energy deposited in a sphere of 50 cm radius around the vertex larger than 1 MeV and a Compton electron multiplicity ≥ 2. Events in this selection which also fulfil the Fermi channel selection are removed from this sample. The resulting efficiency is 57% for Gamow-Teller events, producing 430 events per year (Table 2.1) with a contamination from elastic scattering which is 6% of the number of elastic scattering events and from Fermi absorption which is 19% of the number of Fermi events.

2.1.2 Background estimates

The main source of background for solar neutrino events comes from neutrons produced by natural radioactivity of the materials surrounding the detector (mainly the rocks around the cave). In the 5000 ton ICARUS module, these neutrons are moderated and absorbed in the outer liquid argon layers. For the 600 ton module, it is necessary to have a neutron shield around the detector. We plan to build a shield made of a neutron moderating medium (water or other hydrogenated material) and of a thermal neutron absorber, or a combination of both (polythene, 1% borate polyurethane, etc.).

The background estimates were calculated by A. Borio and M. Terrani [11] using the MNPC-4 code. With, for example, a 65 cm borated polythene shield, we expect to have a total number of background events of 260 with at least one electron of energy larger than 5 MeV. The detailed numbers of background events are listed in Table 2.1, showing that for elastic events the signal over background ratio exceeds 20, for Fermi transition it is 110 and for Gamow-Teller events it is 10.

Table 2.1: Signal and Background rates in a fiducial mass of 540 tons, for the various channels used in the solar neutrino study. The neutron shield used corresponds to one metre of polythene with thermal neutron absorber. The Standard Solar Model of Bahcall et al. [12] was used for the signal prediction.

Reaction	**Signal (events per year)**	**Radioactivity background (events per year)**	**Contamination from other channels per year**
$\nu_x + e-$	290	13	18
ν_e + Ar (Fermi)	330	3	68
ν_e + Ar (G.T.)	430	43	110

There exist other sources of background (from through-going muons, ^{42}Ar decays, the material of the detector itself), they have been discussed in details in our proposal [1] and found to be negligible in the case of the 5000 ton module, they are also negligible for the 600 ton module.

2.2 Measurement of the shape of the ^8B solar neutrino spectrum

2.2.1 The method

We are considering an additional and unique way to provide a solar model independent measurement, by measuring the shape of the ^8B solar neutrino energy spectrum. The combined analysis [19] of the present solar neutrino data provides two possible MSW solutions, one "non-adiabatic" ($\Delta m^2 = 6.2\times10^{-6}$ eV^2; $\sin^2(2\theta) = 6.8\times10^{-3}$), the other "adiabatic" or large mixing angle solution ($\Delta m^2 = 9.7\times10^{-6}$ eV^2; $\sin^2(2\theta) = 0.62$). If the non-adiabatic MSW solution to the solar neutrino problem is relevant, then not only is the rate of ^8B neutrinos affected but the shape of the neutrino spectrum should be significantly distorted. The effect is most spectacular for the so-called "non-adiabatic" solution, which is the most natural one (small mixing) and also the one which fits best the present data.

We note that in the sun, ^8B neutrinos are produced in the β-decay reaction:

$$^8B \rightarrow {}^8Be^* + e^+ + \nu_e \quad (Q_B \sim 14.0 \text{ MeV})$$

whose properties are well known, in terms of ordinary nuclear physics. In particular, the ν_e energy spectrum follows a standard Kurie plot, exhibiting a linear behaviour easy to visualise and to quantify:

$$\left[\frac{1}{E_\nu^2}\frac{dN_\nu}{dE_\nu}\right]^{\frac{1}{2}} \propto \left(Q_B - E_\nu\right)$$

We intend to reconstruct this Kurie plot by making use of the fact that low energy neutrinos have a large cross-section for interaction with neutrons. Therefore, we are considering the possibility of introducing a fraction (≤ 5% in mass) of deuterated methane (CD_4) in the liquid Argon. This provides quasi-free neutrons and results in a scattering kinematics which does not suffer from important Fermi motion smearing (Figure 2.2).

The $\nu_e + d \rightarrow p + p + e^-$ ($Q_D = -1.44$ MeV) reaction used, has an unambiguous signature, an electron up to 12.5 MeV and two protons producing an intense ionisation spot, as shown in Figure 2.1 which was obatined from a Monte Carlo simulation. The cross-section for this reaction increases as E_ν^2 in good approximation and has been calculated by J. N. Bahcall [18]. The interesting feature is that the neutrino energy can be obtained from the total visible energy through $E_\nu = E_{vis.} - Q_D$ and that measuring the end point of the visible energy spectrum, will provide evidence that the reaction producing these neutrinos is actually ^8B decay in the sun. The Kurie plot can be experimentally obtained by plotting the following quantity:

$$K(E_{vis.}) = \left[\frac{\frac{dN}{dE_{vis.}}}{E_{vis.}^2 \left(E_{vis.} - Q_D\right)^2} \right]^{\frac{1}{2}}$$

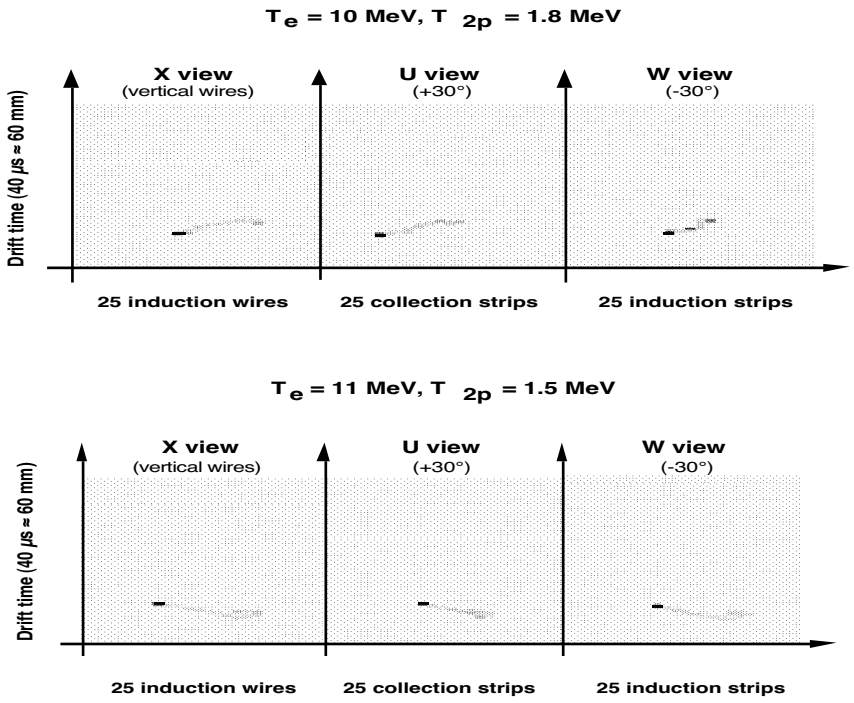

Figure 2.1: Simulation of two solar neutrino scattering events on deuterium. Three views are shown corresponding to one collection and two induction readout planes. The electron kinetic energies are respectively 10 and 11 MeV.

As shown in Figure 2.4, if there is no neutrino oscillations the Kurie plot should follow the expected linear behaviour. If the non-adiabatic solution is relevant, the departure from the straight line is spectacular. It will take 2 to 3 years of data to distinguish the two shapes in an unambiguous way [the errors reported on Figure 2.3 are statistical only]. We must note that the shape of the adiabatic solution does not differ sufficiently from the no-oscillation case to hope to have a rapid answer. However, we have the additional handle of the ratio of rates of reactions (1) and (2) to allow a model independent conclusion, also in the case of the adiabatic solution.

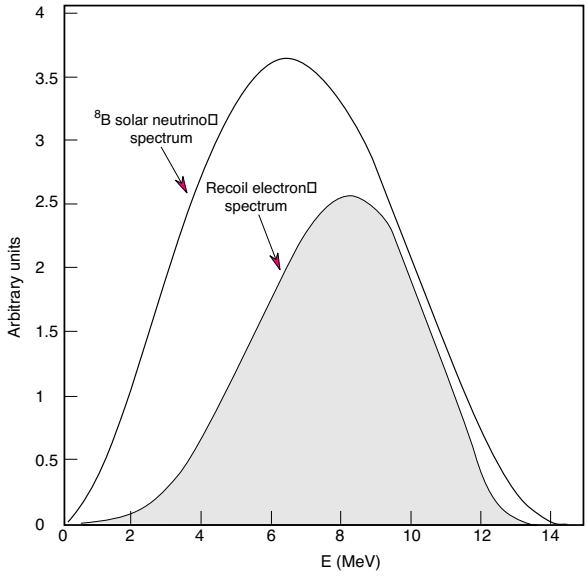

Figure 2.2: ^{8}B solar neutrino energy spectrum and the expected recoil electron energy spectrum in the reaction $\nu_e + d \rightarrow p + p + e^-$ under the hypothesis of no oscillations.

Most of the ^{8}B neutrino energy spectrum is in the range attainable with the ICARUS 600 ton module. In particular, the radioactivity shield which we envisage (water and thermal neutron absorber), should allow us to observe recoil electrons down to 5 MeV or possibly lower.

A rate of 590 events per year is expected for a CD_4 concentration of 5% in mass and for an electron kinetic energy threshold of 4.5 MeV. One can see that, in this case, one collects more than 80% of all ^{8}B neutrinos.

2.2.2 Event Rate and Background estimate

The main source of irreducible background in this case is neutrino scattering on electrons. The requirement of the presence of a high energy density at the beginning of the electron track can reduce strongly this background. However, this background can also be measured precisely in the experiment, by running with different CD_4 concentrations. At the beginning of the run we would start without CD_4, and the selection would collect background only. Then in the run with a certain concentration of CD_4 we will select both signal and background, which can then be subtracted.

Work is in progress to obtain an accurate prediction of the background, however it should be noted again that, in the experiment, the background will be measured precisely, by varying the concentration of CD_4.

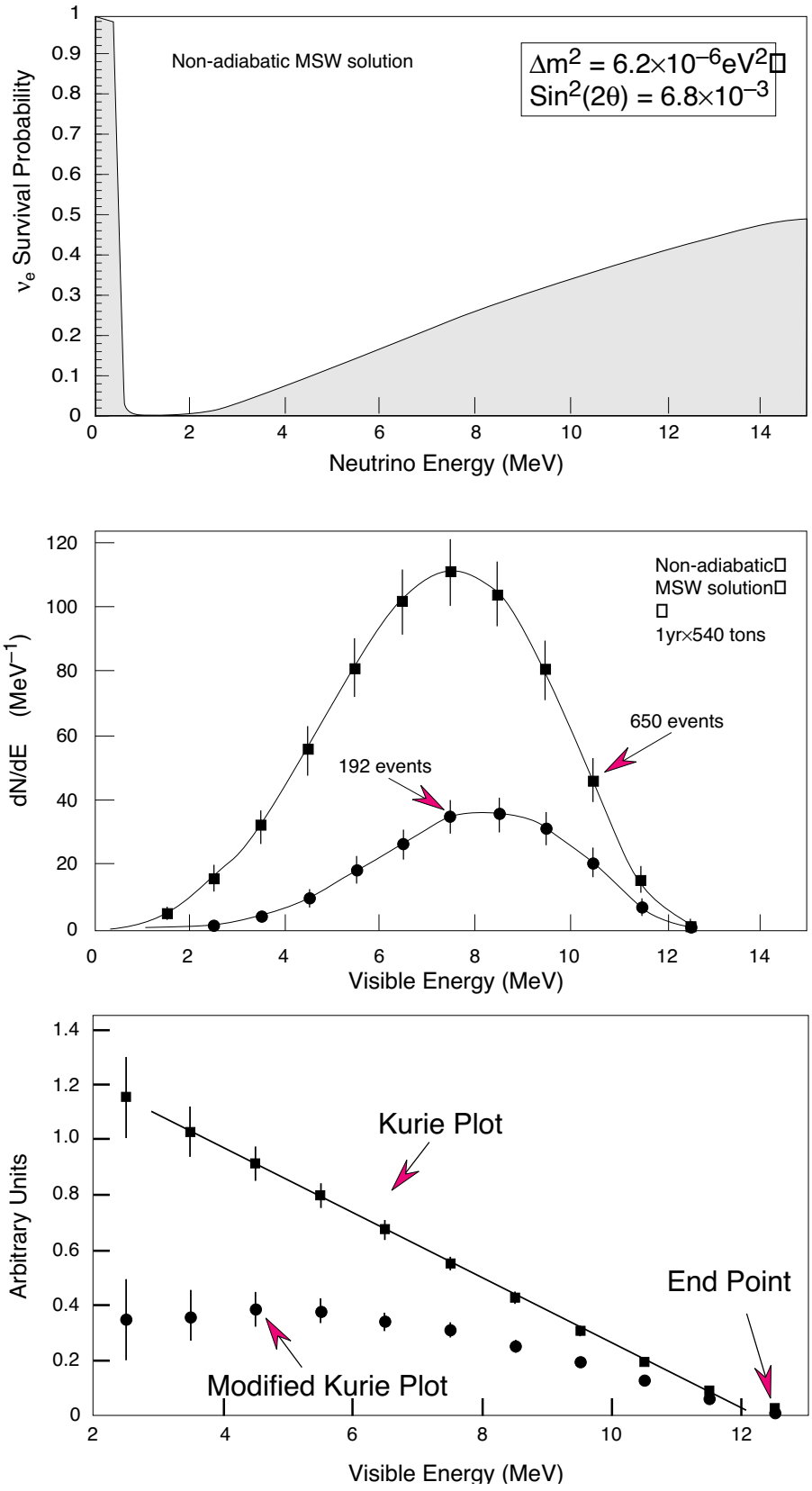

Figure 2.3a: (top) Survival probabilities of solar ν_e's, for the non-adiabatic MSW solution to present solar neutrino data; (middle) Undistorted and MSW modified ^{8}B solar neutrino spectrum; (bottom) Kurie plot and modified Kurie plot .

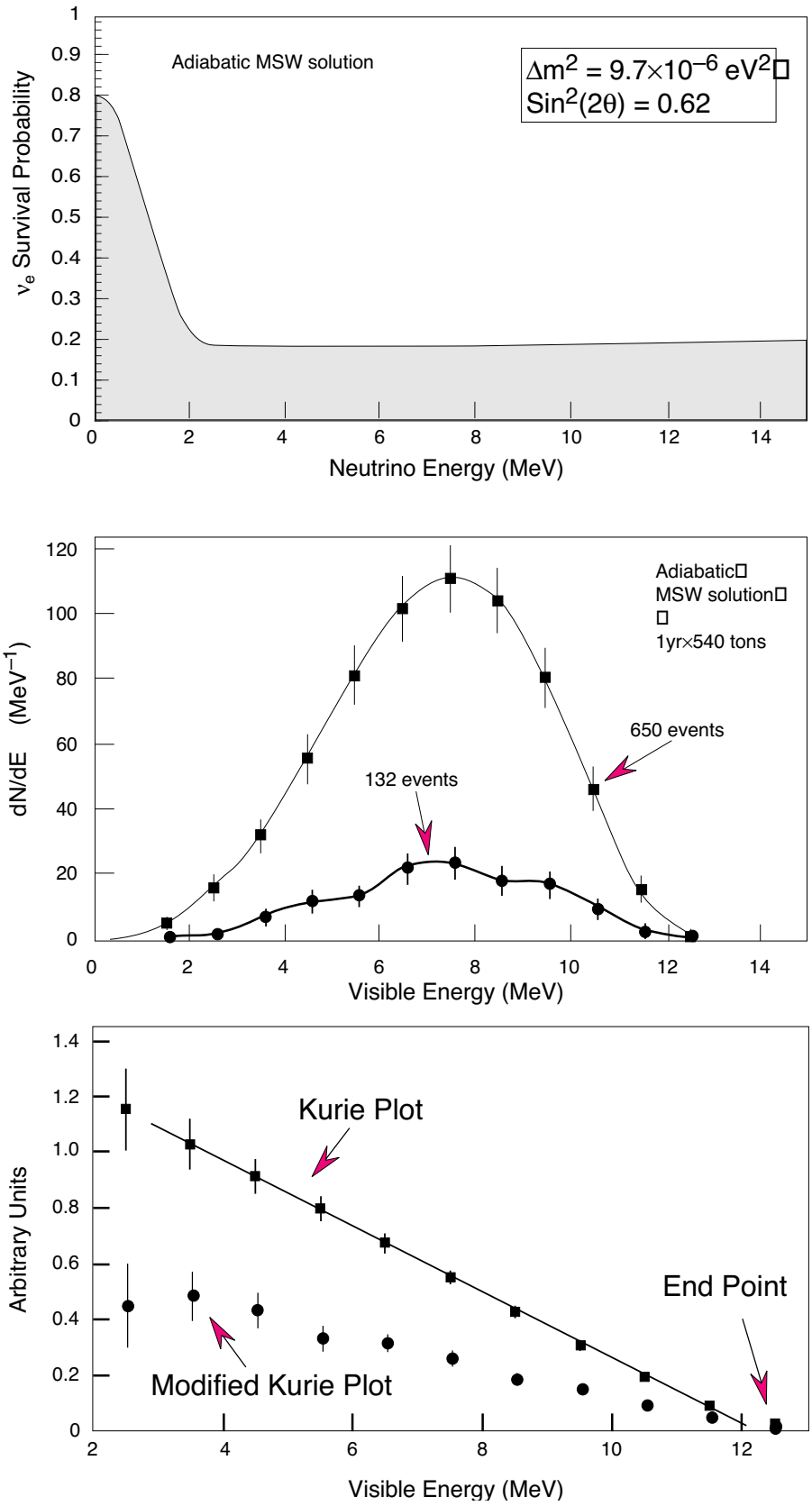

Figure 2.3b: (top) Survival probabilities of solar ν_e's, for the adiabatic MSW solution to present solar neutrino data; (middle) Undistorted and MSW modified ^{8}B solar neutrino spectrum; (bottom) Kurie plot and modified Kurie plot .

2.3 Conclusion on solar neutrino studies with the 600 ton module

In two years, assuming that statistical errors dominate (which is certainly true for elastic scattering and Fermi absorption events) we will be sensitive to relative variations of the ratio of elastic to Fermi absorption events larger than 12% (90% C.L.). The present two MSW solutions to the solar neutrino apparent deficit, correspond to an increase of this ratio between 10 and 50% for the non-adiabatic solution and between 50 and 70% for the adiabatic solution. In two years, if the adiabatic solution is the correct one, we will be able to give a definite confirmation of the solar neutrino oscillation hypothesis, or, if no evidence of oscillations is found, we will exclude the adiabatic solution and most of the non-adiabatic one.

The measurement of the shape of the ^{8}B solar neutrino spectrum, with determination of the end-point of the Kurie plot, will give a direct, unambiguous and Solar Model independent diagnostic of the nature of the solar neutrino problem.

With the 3 mm wire pitch and a robust neutron shield, the 600 ton module at the Gran Sasso Laboratory will allow for a conclusive study of solar neutrinos. ICARUS will not only confront the Standard Solar Model by comparing its predictions to the observed rates of events in three different reactions, it will also, in a model independent way, check whether, in case the neutrino deficit is confirmed, it is linked to neutrino properties or not.

3. Proton decay

Even with a relatively low mass[3] our test module can provide important contributions to the proton decay search, in particular for those decay modes (referred in the following as *exotic decay modes*) with high multiplicities (3 or 4 particles in the final state) or, more generally, with signatures particularly difficult to identify with previously used detector techniques.

One example of such decay modes is $p \rightarrow e^+ \nu \nu$which has been emphasised in our proposal [1] because it can be interpreted as the source [13] of the excess electron-like events in the Kamiokande [3, 5] and IMB [14] experiments. This type of event belongs to a class of decay modes with $\Delta B = -\Delta L$ which is one of the distinguishing features of $SU(4)^{colour}$ Grand Unification Theories. This model has been first proposed by J. Pati and A. Salam in 1973 [15]. Nucleon decays to l + meson(s), to **Error!**) + meson(s) and also to l + l**Error!**) + meson(s) are all possible within the framework of the theory with lifetimes between 10^{30} and 10^{33} years [16, 17] and the relative decay amplitudes for these modes depend on parameters of the model that are not fixed *a priori*. Actually, the present experimental situation seems to disfavour two body decays to **Error!**) + meson with lifetime limits in most of the channels at the level of 10^{32} years or more while for l + meson(s) decays with limits between 10^{31} and 10^{32} years, the situation is still entirely open. For what concerns decays to l + l**Error!**) + meson(s) some candidates have been reported in the past by several experiments (see Ref. [17] and references therein), but a complete analysis has never been published and no limits are available on partial lifetimes, at least at the level of 10^{30} years. This is probably due to the difficulty for these experiments to analyse high multiplicity events.

With its superior characteristics of high space and energy resolution and particle identification capabilities the ICARUS technique will help to fill this gap. With a sensitive mass of about 540 tons the ICARUS prototype can probe in one year lifetimes up to 1.5×10^{32} years. Moreover, this module will have three readout planes and a better space resolution (3 mm^3 instead of 5 mm^3) with respect to the one foreseen for the big ICARUS, and therefore it will be even better suited for the analysis of complicated topologies. In this sense the physics programme of the 600 ton module will be, at least in part, complementary to the one of the full detector.

Table 3.1 reports the rates and the background expected for a 540 ton prototype in some of the channels characteristic of the Pati-Salam model, assuming that the nucleon lifetime is at the current experimental limit.

The ICARUS technique is particularly well suited to identify these decay modes, or any decay mode involving several charged particles in the final state. The detector techniques used so far, especially water Cerenkov

[3] It is worth noticing that our prototype will have a sensitive mass which is comparable to those of the Kamiokande and Frejus experiments.

detectors, do not allow to study these decay modes in an exclusive way, as can be seen from the relatively modest present limits. For most of them the background in ICARUS is expected to be negligible, hence one single event is sufficient for a discovery.

Tables 3.1 and 3.2 also report the detection efficiencies for the various channels. These efficiencies include the requirement that the events are contained in the detector. For nucleon decay events, with the present geometry for the 600 ton module, it turns out that the containment request does not reduce very much the fiducial volume. The fiducial to sensitive mass ratio (given explicitly in parentheses in Tables 3.1 and 3.2) ranges from 0.55 for $p \to \mu^+ \pi^0$ events (whose typical dimension is 2 metres) to 0.88 for $p \to \bar{\nu} K^+$ events (whose typical dimension is 1 metre) to even larger values for higher multiplicity events. Considering that a certain segmentation with relatively large dead zones (for supporting frames, internal electronic boards, etc.) will be probably present also in a single 5000 ton detector, the above consideration favours a strategy of using several 600 ton modules to reach the 5000 ton sensitive mass.

Table 3.1: For a number of exotic decay modes, the detection efficiency (including the fiducial volume cut), the present limits, the rates in the 600 ton module corresponding to the present limit are given.

Decay Mode	**Efficiency**	**Present Limit (10^{31} years)**	**Events (year^{-1})**
$p \to e^- \kappa^+ \pi^+$	0.36 (.9)	2.0	2.6
$p \to \mu^- \kappa^+ \pi^+$	0.36 (.9)	0.5	10.5
$p \to \mu^+ \kappa^0_S$	0.72 (.8)	6.4	1.7
$p \to \mu^+ \kappa^0_L$	0.29 (.7)	4.4	1.0
$p \to e^- \pi^+ \pi^+$	0.12 (.9)	3.0	0.59
$p \to \bar{\nu} \pi^+$	0.36 (.85)	2.5	2.0
$p \to e^+ \nu\nu$	0.72 (.85)	1.1	9.6
$p \to \mu^+ \nu\nu$	0.68 (.8)	2.1	4.7
$n \to e^+ e^- \nu$	0.72 (.8)	7.4	1.8
$n \to e^- \pi^+$	0.30 (.75)	6.5	0.83
$n \to \mu^- \pi^+$	0.26 (.7)	4.9	0.91
$n \to \mu^- e^+ \nu$	0.54 (.6)	4.7	2.1
$n \to e^- \kappa^+$	0.68 (.8)	3.2	3.8
$n \to \mu^- \kappa^+$	0.64 (.75)	5.7	2.0
$n \to e^- e^+ e^- \pi^+$	0.36 (.9)	0.1	12
$n \to e^- e^+ e^- \kappa^+$	0.81 (.9)	0.1	27
$n \to \mu^- e^+ e^- \pi^+$	0.36 (.9)	0.1	12

$n \to \mu^- e^+ e^- \kappa^+$	0.81 (.9)	0.1	27

Table 3.2 reports the rates and the background expected for a 540 ton module in the channels already reported in our proposal [1].

Table 3.2: For a number of standard decay modes, the detection efficiency (including the fiducial volume cut), the present limits, the rates in the 600 ton module corresponding to the present limit and the expected background are given.

Decay Mode	**Efficiency**	**Present Limit (10^{31} years)**	**Events (year^{-1})**	**Background (year^{-1})**
$p \to e^+ \pi^0$	0.25 (.6)	55	0.07	$< 2 \times 10^{-2}$
$p \to \bar{\nu} \pi^+$	0.36 (.85)	2.5	2.0	1.4
$p \to \mu^+ \pi^0$	0.21 (.55)	27	0.12	$< 2 \times 10^{-2}$
$p \to \bar{\nu} \kappa^+$	0.60 (.88)	10	0.9	$< 5 \times 10^{-3}$
$p \to e^+ \pi^+ \pi^-$	0.12 (.9)	2.1	0.83	$< 2 \times 10^{-2}$
$p \to e^+ \rho^0$	0.07 (.9)	7.5	0.14	$< 2 \times 10^{-2}$
$p \to e^+ \nu\nu$	0.72 (.85)	1.1	9.6	0.43
$p \to e^+ e^- e^+$	0.64 (.8)	51	0.19	$< 2 \times 10^{-2}$
$n \to e^+ \pi^-$	0.3 (.75)	13	0.37	$< 2 \times 10^{-2}$
$n \to \mu^+ \pi^-$	0.26 (.70)	10	0.46	?
$n \to \nu \pi^0$	0.31 (.75)	10	0.57	?
$n \to e^- \kappa^+$	0.68 (.8)	3.2	3.8	$< 2 \times 10^{-2}$
$n \to e^+ \rho^-$	0.07 (.9)	5.8	0.22	?
$n \to e^+ \pi^- \pi^0$	0.10 (.75)	3.2	0. 53	?
$n \to \nu \kappa^0$	0.53 (.8)	8.6	1.1	$< 2 \times 10^{-2}$

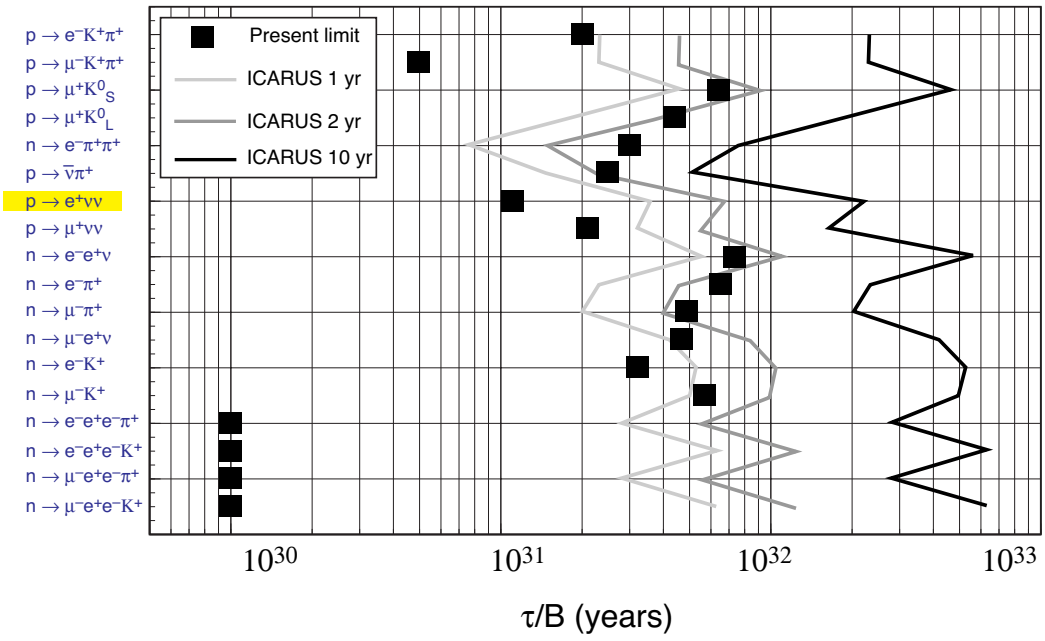

Figure 3.1: Present limits for a number of "exotic" proton and neutron decays together with the 90% ICARUS sensitivity, with the 600 ton module and for data taking periods of 1, 2 and 10 years.

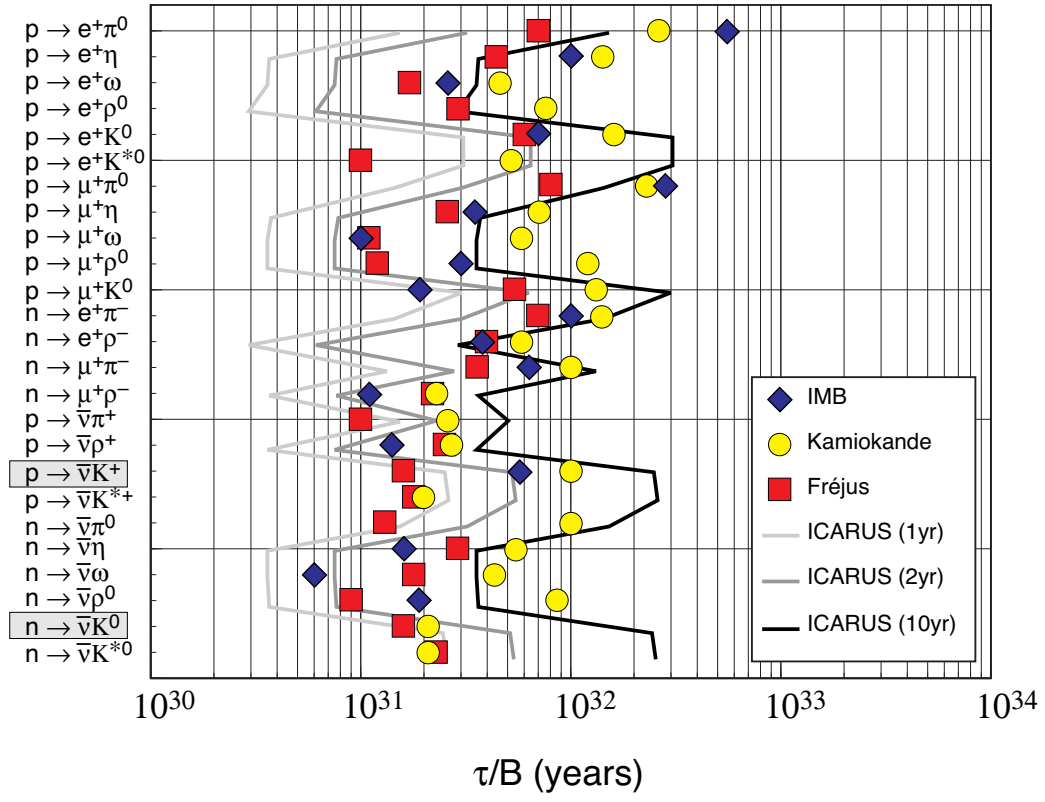

Figure 3.2: Present limits for a number of "standard" proton and neutron decays together with the 90% ICARUS sensitivity, with the 600 ton module and for data taking periods of 1, 2 and 10 years.

With our 600 ton module, in a few years, we will be able to explore a lifetime region exceeding 10^{32} years for most of the channels reported in the

above tables, with a considerable improvement (a factor 5 to 100) of the present limits for the exotic channels (see Figure 3.1). It is clear that with one single module we cannot reach the lifetime limit of 10^{34} years (Figure 3.2) which is needed to fully test the minimal SUSY Gran Unification Theory and which is the final goal for the 5000 ton detector. We nevertheless will satisfy completely what is our requirement for this first phase of our programme and namely to extend the present knowledge of the nucleon stability over the widest possible range of decay modes at the same level of the presently best studied channels.

4. Long baseline neutrinos

The beam simulation studies have shown that the highest proton energy is preferable if one wants to maximise the number of events in the detector. If we assume that the beam can produced in one year 2×10^{19} 450 GeV protons from the CERN SPS, the ideal focusing gives 600 ν_μ charged current events in one year per 100 ton. In a realistic focusing scheme (very similar to the one presently working at CERN), we expect 160 ν_μ charged current events and 0.96 ν_e charged current event in one year per 100 ton. The corresponding number of neutral current events is 50. Since the mean energy of the charged current events is around 30 GeV, in order to allow for the complete containment of the events within the detector sensitive volume, we have defined a mean fiducial volume for long base line neutrino interactions of ≈ 350 tons. It follows that the corresponding total rate is about 735 events per year.

Contained event rates (fiducial volume of 350 ton) in one year

	Ideal Focus	**Realistic focusing**
$\langle E_\nu \rangle$ (GeV)	40	30
ν_μ C.C. events	2100	560
ν_e C.C. events	6.3	3.4

Sensitivity to oscillations for one year (fiducial volume of 350 ton), and for the two following oscillation hypotheses:

$\nu_\mu \leftrightarrow \nu_e$	**Ideal Focus**	**Realistic focusing**
Δm^2	2.3×10^{-3}	3.0×10^{-3}
$\sin^2(2\theta)$	5.7×10^{-3}	1.8×10^{-2}

$\nu_\mu \leftrightarrow \nu_\tau$	**Ideal Focus**	**Realistic focusing**
Δm^2	6.8×10^{-3}	7.3×10^{-3}
$\sin^2(2\theta)$	5.3×10^{-2}	1.0×10^{-1}

The above limits are based on statistical methods only. For $\nu_\mu \leftrightarrow \nu_e$, in one year, the sensitivity is sufficient to cover entirely the Kamiokande allowed region of the Δm^2 vs $\sin^2(2\theta)$ plane (Figure 4.1). For $\nu_\mu \leftrightarrow \nu_\tau$, in one year a good fraction of the region of interest is covered, in particular the best fit value (Figure 4.1), and in two to three years the region of interest would be entirely covered.

If it turned out that ICARUS confirms the existence of oscillations from the study of atmospheric neutrinos, it would be of great interest to use the long base line neutrino beam, which gives sensitivity to the same region of the oscillation parameter plane, but with a much smaller systematic error since the main source of systematics is the ν_e contamination of the beam. In this case we could tune the neutrino energy spectrum of the beam in order to enhance the sensitivity in the desired oscillation parameter region. If, with the

beam, we obtain a significant signal, we will then be able to tell whether the oscillations observed in the atmospheric neutrino case are $\nu_\mu \leftrightarrow \nu_e$ or $\nu_\mu \leftrightarrow \nu_\tau$.

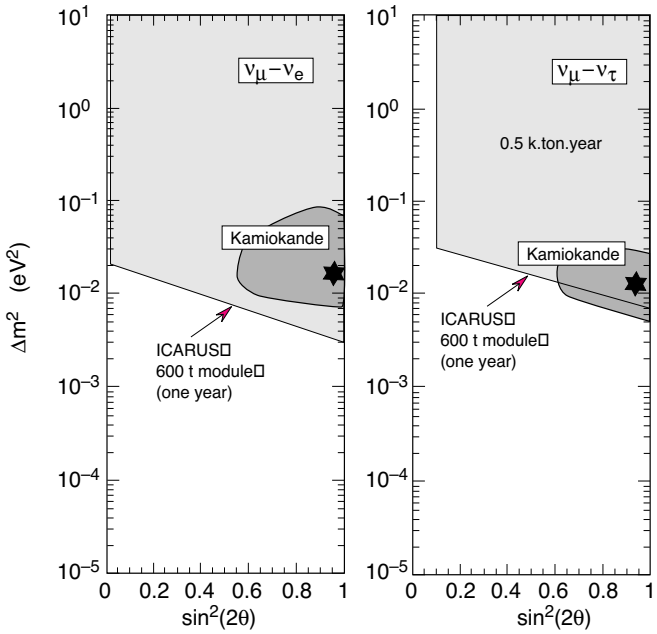

Figure 4.1: Sensitivity of ICARUS with the 600 t module to $\nu_\mu \leftrightarrow \nu_e$ and $\nu_\mu \leftrightarrow \nu_\tau$ oscillations, for one year of data.

In conclusion, the CERN neutrino beam would be a very important contribution to resolving the possible atmospheric neutrino puzzle. As soon as the CERN neutrino beam is available, ICARUS, with the 600 ton module, will be ready to use it.

References

[1] The ICARUS Collaboration, "*ICARUS II, a second-generation proton decay experiment and neutrino observatory at the Gran Sasso Laboratory*", LNGS - 94/99 Vol. I & II, Proposal.

[2] P. Cennini et al., Nucl. Instr. and Meth. in Phys. Res. A345 (1994) 230-243.

[3] K. S. Hirata et al., Phys. Lett. B280 (1992) 146-152; Phys. Rev. Lett. 65 (1990) 1297.

[4] R. Davis Jr., BNL-508-79, "The Status and Future of Solar Neutrino Research", (1978) 1, ed. G. Friedlander; Proc. Works. on Neut. Telescopes, ed. M. Baldo-Ceolin, Palazzo Loredan, Venice, Feb. 1990, pp 1-13.

[5] Y. Fukuda et al. Phys. Lett. B 335 (1994) 237.

[6] O. Ryazhskaya, "Is there an excess of electron neutrinos in the flux in the atmosphere?", JETP Lett. Vol. 60, No. 9 617-620 (10 Nov. 1994).

[7] G. Barr, T. Gaisser and T. Stanev, Phys. Rev. D39 (1988) 85; T. Gaisser and T Stanev, Phys. Rev. Lett. 51 (1983) 223.

[8] GENEVE Monte Carlo, developed by the ICARUS Collaboration, described in Ref. [1], Vol. I, section 2.3.2), write-up in preparation.

[9] S. K. Singh and E. Oset, Nucl. Phys. A542 (1992) 587-615.

[10] CERN - Harvard - Milano - Padova - Roma - Tokyo - Wisconsin - Collaboration, "Searching for New Underground Phenomena with High Resolution Visual Techniques and Magnetic Analysis", Proposal for the Gran Sasso Laboratory, INFN/AE - 85/7 Frascati (1985).

[11] A. Borio and M. Terrani, private communication.

[12] J. N. Bahcall and M. H. Pinsonneault, Rev. of Mod. Phys. 64 (1992) 885.

[13] W.A. Mann, T. Kafka and W. Leeson, Phys. Lett. **B291** (1992) 200.

[14] D. Casper et al., Phys. Rev. Lett. 66 (1991) 2561.

[15] J.C. Pati and A. Salam, Phys. Rev. Lett. **31** (1973) 661.

[16] J.C. Pati, A. Salam and U. Sarkar, Phys. Lett. **B133** (1983) 330.

[17] J.C. Pati, Phys. Rev. **D29** (1984) 1549.

[18] J.N. Bahcall, "Neutrino Atrophysics", Cambridge University Press, 1989.

[19] N. Hata, "Solar Neutrinos: Hint for Neutrino Mass", UPR 0612 T/9420, Proc. Solar Modeling Workshop, Institute of Nuclear Theory, U. of Washington, Seattle, March 24, 1994.

III. CONSTRUCTION OF A 600 TON MODULE

1. Introduction

The intermediate step to the final 5000 ton detector has to be designed in such a way that the solutions implemented on it (for safety, mechanics, cryogenics, etc.) can be extrapolated with large confidence and in the most straightforward way to the final detector. Since it will require in any case a relatively large effort either in terms of money and time it is somewhat necessary to capitalize this work also with some physical outcome. The most natural choice, which is also compatible with the program for the 5000 ton detector, is to redo and extend, with this module at the Gran Sasso Laboratory, the physics that has been done in the past by experiments like Kamiokande and IMB and check with a different and better technique if their results on solar and atmospheric neutrinos are correct. As a consequence the mass of the prototype should approach as much as possible one of the above experiments.

As a general strategy we decided that the most time efficient and economical way to have the intermediate module operative is to build and test it outside the Laboratory and then take it to the Hall C for the final assembly. This implies that the module has to be transportable.

It turns out that the single largest transportable object on the Italian highways and into the Hall C has a volume which corresponds to a fiducial mass of about 250 tons which is too small for the physics we intend to do. Consequently we have been obliged to split our volume. The present design foresees two identical semi-independent half-vessels with dimensions that correspond to the maximum transportable.

In order to fit the geometry of the entrance doors to the Gran Sasso Laboratory, the cross-section of the half-vessels has to be approximately squared. Although not the best solution from the mechanical point of view this geometry has a pleasant outcome. The read-out chambers (two for each half-vessel) can be mounted on the internal walls of the dewar with the cathode at the centre with a simplification of the sustaining structures of the chambers and an enlargement of the fiducial volume (as the cathode is now automatically far from the grounded walls).

We opted for a passive insulation of the dewar instead of the vacuum insulation that was foreseen for the 5000 ton detector. Passive insulation has two main advantages over vacuum insulation: first, it eliminates completely the risks coming from a vacuum breaking, and second, it allows for the internal cold vessel to be transported alone with an increase, for equal external dimensions, of the internal volume.

The mounting strategy for the 600 ton module will proceed through the following steps: the detector will be completely mounted and tested outside the Gran Sasso Laboratory, it will then be evacuated of the liquid argon, the passive insulation (blocks of preformed foam or, as suggested by

Air Liquide, modules of honeycomb flushed with nitrogen gas) will be removed, the two half-vessels will be separated and will be independently transported into the Hall C. The final assembly of the external insulation and the construction of the neutrons shield, will be the only two major works that will be performed inside Hall C.

In the following sections we will give a description of those technical items that are specific of the 600 ton module (dewar, cryogenics, general layout, etc.). As modularity has been one of the guidelines for the project of the ICARUS detector we heavily based the present design of the 600 ton prototype on what has been described in detail in our technical prototype.

2. Preliminary dewar design

We present here a possible solution for the detector dewar and the cryogenic system of the 600 ton module. The design is obviously still preliminary but it can be considered already accurate at least for what concerns the main project parameters (dimensions, loads, acceptable stresses, heat losses, general layout). The final solution will be decided together with the manufacturing industries during the engineering phase.

2.1 Mechanics

As described in the previous 5000 ton Technical Report also the 600 ton is the result of our co-operation with the office of Progetti Industriali di R. Giannone & C. As mentioned in the introduction, the 600 ton module has been conceived in two C-shaped semi-independent and symmetric halves giving a rectangular cross-section, whose dimensions are limited by the transportability on the Italian highway network and inside the GS Laboratory.

The main design parameters, the geometrical characteristics and the applied loads are presented in Tables 1 and 2.

The LAr cryogenic container tank is made of Stainless Steel 304L and is completely surrounded by a 60 cm insulation layer (Figure 1).

The two opposed C-halves are connected with walls in tight cool contact, whose joint has been accurately designed (Figure 1). The inner lateral and central walls will be designed to support also the TPC wires tension applied directly on them.

As the vessel shrinks during the cooling phase, the support devices have to follow the adjustment, keeping their functionality unchanged. For this purpose, the support devices have been designed with hinges at one end to allow for free movement along the shrinking direction.

Table 1: Design loads[1].

Design pressure	1.48 bar abs
Working pressure	1.2 bar abs
Hydrostatic pressure on the bottom	0.51 bar
Maximum overpressure on the bottom	0.51 + 0.48 bar
External overpressure (vacuum)	1 bar
Design temperature	83 K
Working temperature	89 K
Tunnel temperature	+ 6°C
Filling liquid	LAr
Undulatory and vertical seismic action	S = 9

Table 2: Main geometrical characteristics of the cold vessel[2]. Data in the table refer to the full 600 ton module with the two half-vessels coupled together.

Internal length	18 200 mm
Internal width	7 056 mm
Internal height	3 625 mm
Total external length	18 840 mm
Total external width	7 800 mm
Total external height	4 175 mm
Half-vessel own weight	≈ 71 t
Total module own weight	≈ 142 t
Internal volume	466 m^3
Volume occupied by LAr	432 m^3
Volume occupied by the Internal Detector structures	34 m^3
LAr own weight	600 t
Sensitive LAr mass	530 t

[1]The criteria adopted in the computations are in conformity with the present rules for the constructions in a seismic area. For the tension determination we have adopted the admissible tension method.

[2]For LAr container we have considered AISI 304L stainless steel laminates and sections, and for the supports and the spacers G11 Vetronite laminates.

One end cup wall of each half-vessel is completely removable to allow for the internal detector installation and eventual inspection and repair. To ensure the vacuum tightness the end cup will be welded to the main body by means of two thin stainless steel lips. The mechanical tight coupling is guaranteed by properly designed clamps.

2.2. Cryogenics

2.2.1 Thermal insulation

As anticipated in the introduction of this section we opted, for the 600 ton module, for a passive insulation. We will describe here a particular solution that has been proposed by technicians from the Air Liquide industry in the course of a series of meetings that we had with them in trying to figure out the most practical choices for the construction and handling of our cryostat.

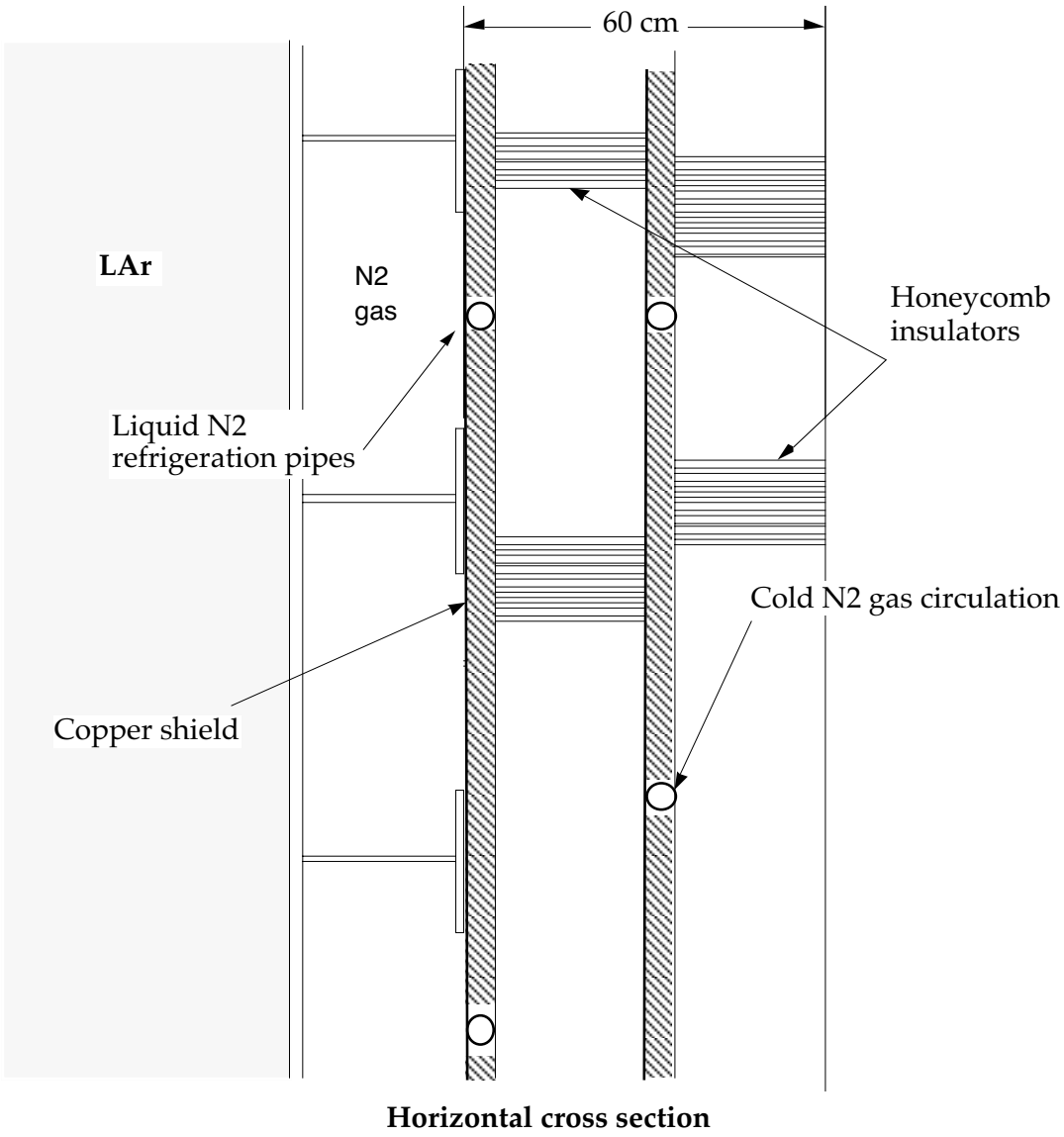

Figure 2: Schematic view of the cooling and insulation systems.

The proposed solution foresees the use, for the external insulation, of modules of honeycomb structures flushed with Nitrogen gas (GN2) (Figure 2). The cross-section of the honeycomb cells is such that convection motions inside the cells are completely blocked; the heat exchange is therefore dominated by conduction through the insulating gas. For a 60 cm layer, taking also into account losses through feed-throughs, passages, etc., we have a mean heat exchange of about 12 W m^{-2}. This figure can be lowered by 25-30% if we use cold GN2 recovered from the cooling system of the detector dewar (see paragraph 2.2.2) to cool a shield in the intermediate part of the honeycomb layer. Taking into account this extra factor the heat losses through the dewar walls are about 4 kW. The power saving obtained with this last solution has however to be evaluated against the complication and the cost of an additional GN2 circuit.

The proposed solution has the advantage of a relative ease of use: the honeycomb insulation can be transported in modules which are then easily assembled or disassembled. Solutions using powders would necessitate the construction on site of a container surrounding the whole LAr dewar. Preformed foams have performances and ease of use which are similar to those of honeycomb at a cost which is eventually much lower. Their use is nevertheless presently disfavoured because of the fact that their contraction coefficient is much bigger than the one of AISI 304L. This point needs however a more careful investigation. The final decision will be taken after a detailed evaluation of all the possibilities taking also into account the relative cost.

2.2.2 Cooling system

As it was conceived for the 5000 ton detector, the cooling of the 600 ton module is provided by two independent sources. The first is a circuit of LN2 at 3.2 bar surrounding the LAr container and the second one is constituted by the recirculation units (operating only during the normal detector running). The relative amount of power subtracted from the system by each of these two devices depends on the rate of recirculation needed to keep the necessary LAr purity and presently has to be considered as a free parameter. A series of tests are in course using our 3 ton prototype at CERN devoted to the clarification of this point.

In this paragraph we will describe in some details the cooling LN2 circuit; a few details about the recirculation units are given in the following section on purification, while a deeper discussion on this last subject can be found in the technical part of our proposal [1].

Figure 3 shows a schematic view of the LN2 cooling circuit together with the system used for the control of the temperature during the initial detector cooling. The cooling circuit consists of a series of rings made of 4 cm diameter pipes surrounding the whole LAr vessel. LN2 is injected at the bottom of the dewar and the produced GN2 will cool a shield located in the middle of the honeycomb insulating layer and will be, at the end, injected in the Hall C ventilation system.

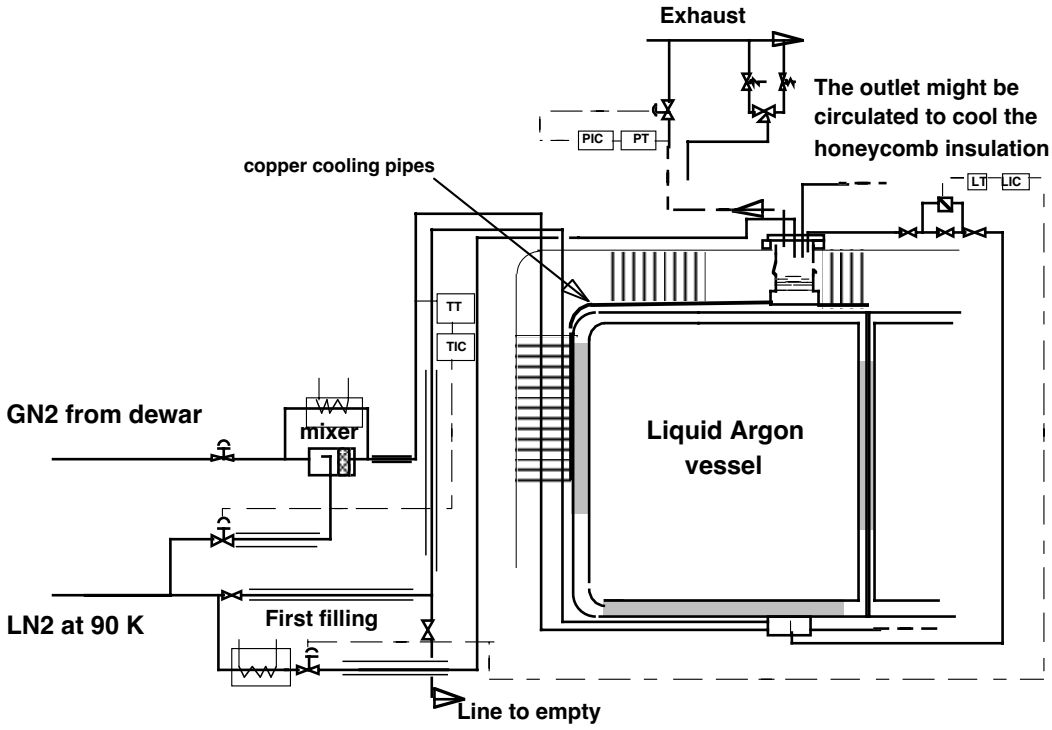

Figure 3: Schematic view of the 600 ton module cooling system.

The pipes of the cooling system are welded on a series of copper plates (to ensure a good thermal contact) which are in turn mounted on the external part of the T-shaped ribs of the LAr vessel (Figure 2). The interspace between the copper plates, the T-shaped ribs and the internal containment skin is filled with GN2. With respect to the scheme with the pipes in direct contact to the internal skin, this solution ensures a more uniform temperature distribution. It will also provide a shield against a direct LAr heating. A localized heat loss (for example through a crack into the insulating layer) would produce boiling in the LN2 circuit with no influence on the stability of the internal LAr system.

During the initial cooling, the cooling circuit will be filled first with cold GN2 and then with LN2. The initial cooling will proceed smoothly enough to avoid unwanted stresses on the vessel and on the various parts of the internal detector. As it has been foreseen for the 5000 ton detector, prior to start the cool down, the 600 ton module will be filled with GAr at 1.2 bar. The Argon atmosphere, whose pressure will be kept constant during all the cooling phase, will ensure a uniform thermalization also of those components of the internal detector which are not in direct contact with the dewar walls. Figure 3 shows a possible scheme for a device that regulates the temperature of the GN2 inside the cooling circuit. Two independent lines, one of GN2 at 300 K and the other of LN2, feed a mixer. The relative amount of warm GN2 and LN2 in the mixture is regulated by an automatic control (TIC) which is operated by a temperature transmitter (TT) placed at the exit of the mixer. The cool down will proceed in steps, a series of sensors placed at the critical points of the device (joints, wires, etc.) will indicate when the desired uniformity in temperature is reached and when the next step can start. We

estimate that the initial cooling will take about 10 days (a decreasing rate of 1-2 degrees per hour). The amount of LN2 needed to cool down the cryostat will be at least 100 m^3.

Table 4 summarizes the heat losses of the 600 ton module during the normal detector operation and includes the heat production due to the presence of the internal electronics (~ 6 x 10^4 channels). A total of about 10 kW have to be provided by the cooling system (LN2 circuit + recirculation units); this corresponds to a consumption of about 8 m^3 per day of LN2 (one truck per day).

Table 4: Summary of the heat losses for the 600 ton module

Source	Heat losses (W)
Walls	4000
Internal electronics	5000
Cables	1000
Total	**10000**

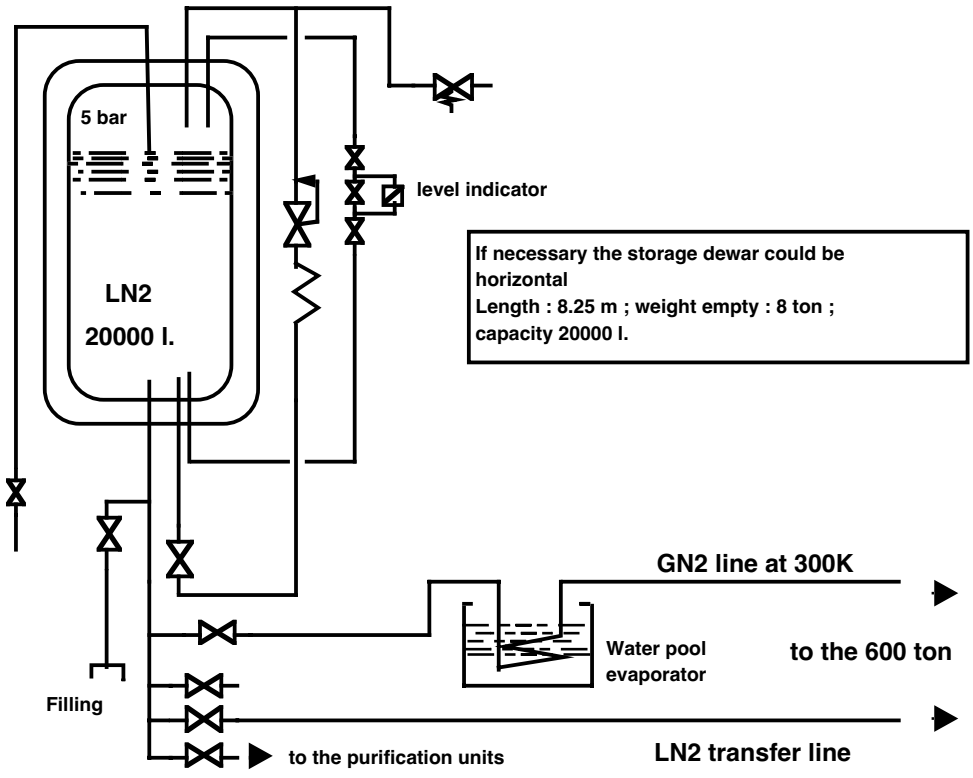

Figure 4: Scheme of the Nitrogen distribution to the various cooling devices.

We foresee to have, in the Hall C, two storage tanks of 20000 litres each, one for LN2 and the other for LAr. The 20000 litres LN2 storage tank will supply Nitrogen to the various devices (Figure 4): LN2 to the cooling

circuit and the purification units, GN2 for flushing the honeycomb insulation. It will ensure an autonomy of about three days in case of delays or other problems on the normal LN2 supply. The LAr storage tank will be kept, during the normal detector operation, empty and will be possibly used, in case of emergency to dump part of LAr from the detector and speed up the emptying operation.

3. Argon purification

The purification procedures for the 600 ton module will be identical to those that have been foreseen for the 5000 ton detector. We give here a few notes and schemes that are specific of the 600 ton module, for all details refer to the appropriate section of the technical part of our proposal [1].

3.1 Pre-filling procedures

At present we foresee to clean, during and after the final assembly, all the components of the internal detector using standard UHV procedures; the internal surfaces of the dewar will be electrochemically polished after the assembly. All these operations are relatively heavy and costly, it might be possible that they will not be necessary (the initial ultra pure GAr + vacuum cycles may be sufficient - see ref. [1] Vol. II pages 41-42) and that can be substituted with normal vacuum cleaning procedures. We plan to perform a test in our 3 ton prototype before the end of the year (during the test of the new read-out chambers) to clarify this point.

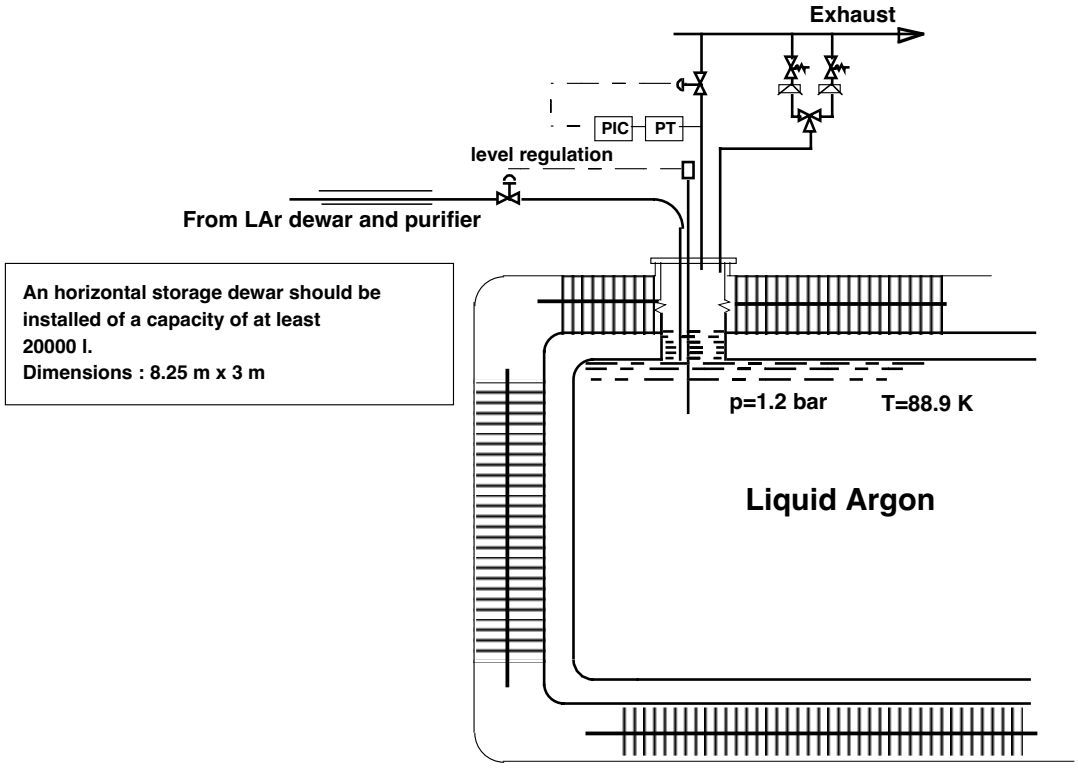

Figure 5: Scheme of the LAr filling circuit

3.2 LAr purification during the first filling

During the first detector filling the Argon will be purified in the liquid phase. Two units, one for each half-vessel, like those described in our technical proposal will be used. To purify the whole detector LAr mass (600 ton) about 6 Oxisorb^{TM} + Molecular sieves cartridges will be necessary. Assuming that the purification rate will be 800 lt/hour/unit, the detector filling will require about ten days.

The same purification units, operated in the gas phase, will be used to purify the Argon during the initial GAr + vacuum cycles. During the normal detector operation these units might stay attached to the internal container on a closed circuit. They will be used to recover quickly the LAr purity (acting as recirculators in the liquid phase) in case of a sudden degradation. Two pumps for cryogenic liquids will be used to insure the liquid recirculation (see ref. [1] Vol. II pag. 44).

3.3 Continuos LAr purification

Figure 6 shows a schematic view of a recirculation unit.

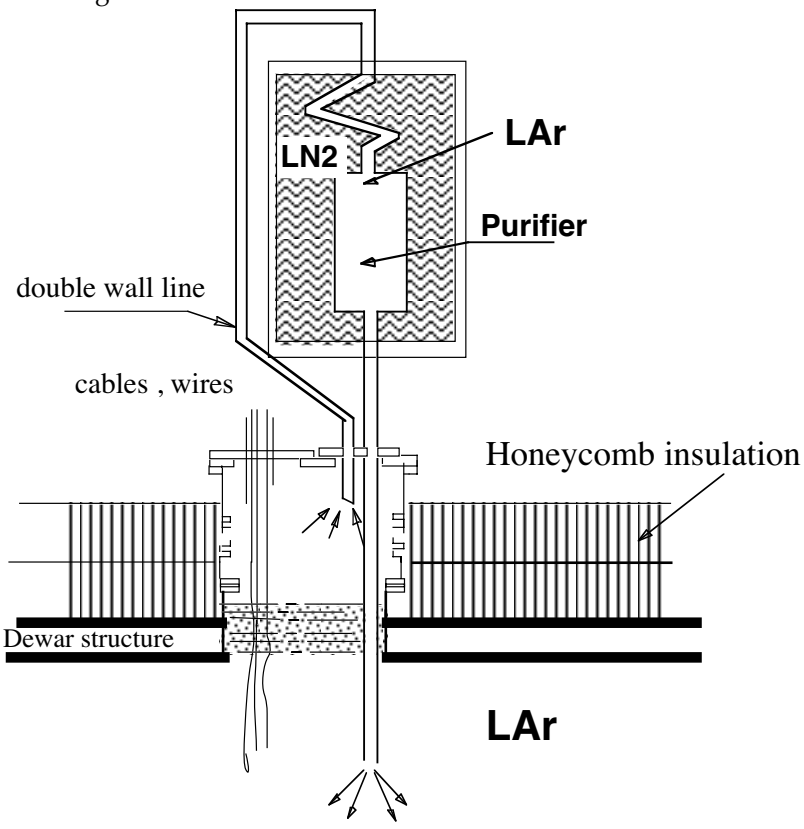

Figure 6: Scheme of a recirculation unit.

The GAr to be purified is taken from the top part of each signal flange[3], it is then recondensed in a LN2 bath and purified in standard Oxisorb^{TM} cartridges. The LN2 bath will stay at 2.7 bar (87 K); this will give a pressure difference between the condenser and the LAr container of about 0.5 bar; enough to compensate for drops along the line and guarantee a

[3]We recall that impurities degassing takes place in the gas phase. Due to the large exposed surface, most of the impurities come from the chamber connecting cables.

sufficient GAr flow. Possibly the rate of recirculation can be increased by removing the copper shield from the cooling system in the upper part of the detector.

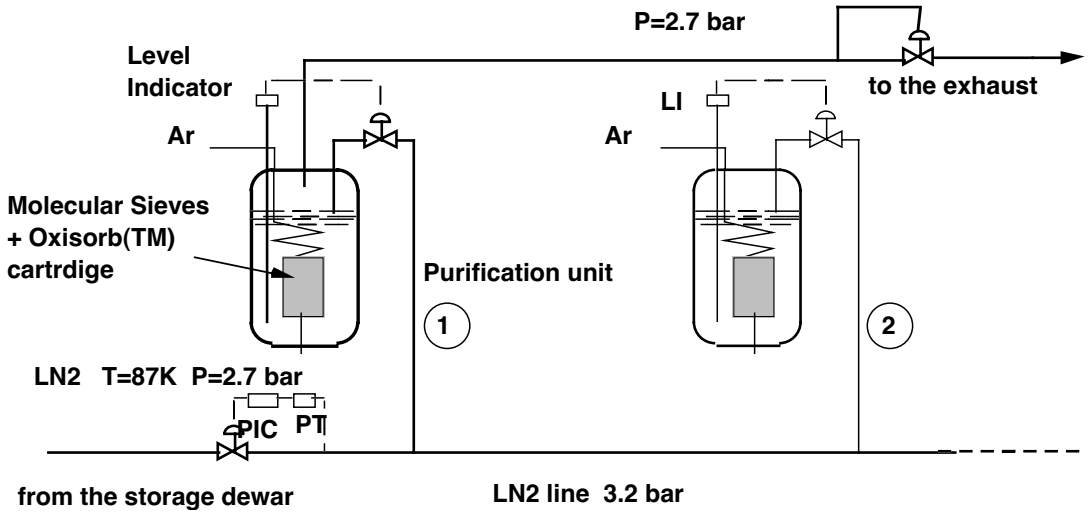

Figure 7: Layout of the recirculation units.

4. Safety issues

In this scaled-down version of the ICARUS detector both Maximum Possible Accident (MPA) and Maximum Credible Accident (MCA)[4] obviously present much less severe consequences than those described in the previous 5000 ton technical proposal. Referring to our proposal, the only possible dangerous events are failure of the cooling system and leaks during the filling operations. In the second case only a small amount of LAr is expected to flow out, much less than one m^3, easily handled as described in the 5000 ton technical report. The failure in the cooling system will transform the cryostat into a passive system. As a consequence, LAr would begin to boil off and the Argon gas phase to overpressurize. Emergency pumps and generators will be installed to drive LN2 from the external tank preventing this occurrence for at least some days, enough to terminate the repairs. If this should not happen, LN2 cold line emergency refilling could go on indefinitely. In the worse case, the exhaust valves break-down will be easily controlled by the emergency ventilation, preventing Ar gas to accumulate in Hall C or to diffuse outside the hall.

Finally, to prevent the LAr flow on the Hall C floor in the case of leaks from the cryogenic tank, the volume under the vessel, around its support system, will be closed for LAr containment. The dimensions of the cryogenic tank are small enough to unload LAr (with about 20 cryogenic trucks) in few days and to provide the necessary repairs.

5. Internal detector.

[4]See the safety section of our technical proposal [1] for the definition of MPA and MCA.

Here follows the main parameter list of the 600 ton prototype.

Overall dimensions of 600 t detector	9000x6225x20040	mm^3
External dimensions of the cold vessel	(2x3900)x4175x18840	mm^3
Internal volume	(2x3528)x3625x18200	mm^3
Total LAr mass	600	ton
Sensitive mass	530	ton
Nr. of independent co-ordinates (with reference to the vertical axis : -45°; +45°; 0°)	3	
Pitch :		
- induction strips	3	mm
- collection strips	3	mm
- induction wires	$3\sqrt{2}$	mm
Total nr. of read-out channels	55420	
- induction strips	19520	
- collection strips	19520	
- induction wires	16384	
Maximum drift length	1640	mm
Maximum H.V. (500V/cm; 300 V/cm)	82 (50)	kV
Nr. of H.V. feed-throughs	16 (8x2)	
Nr. of signal feed-throughs flanges	112	

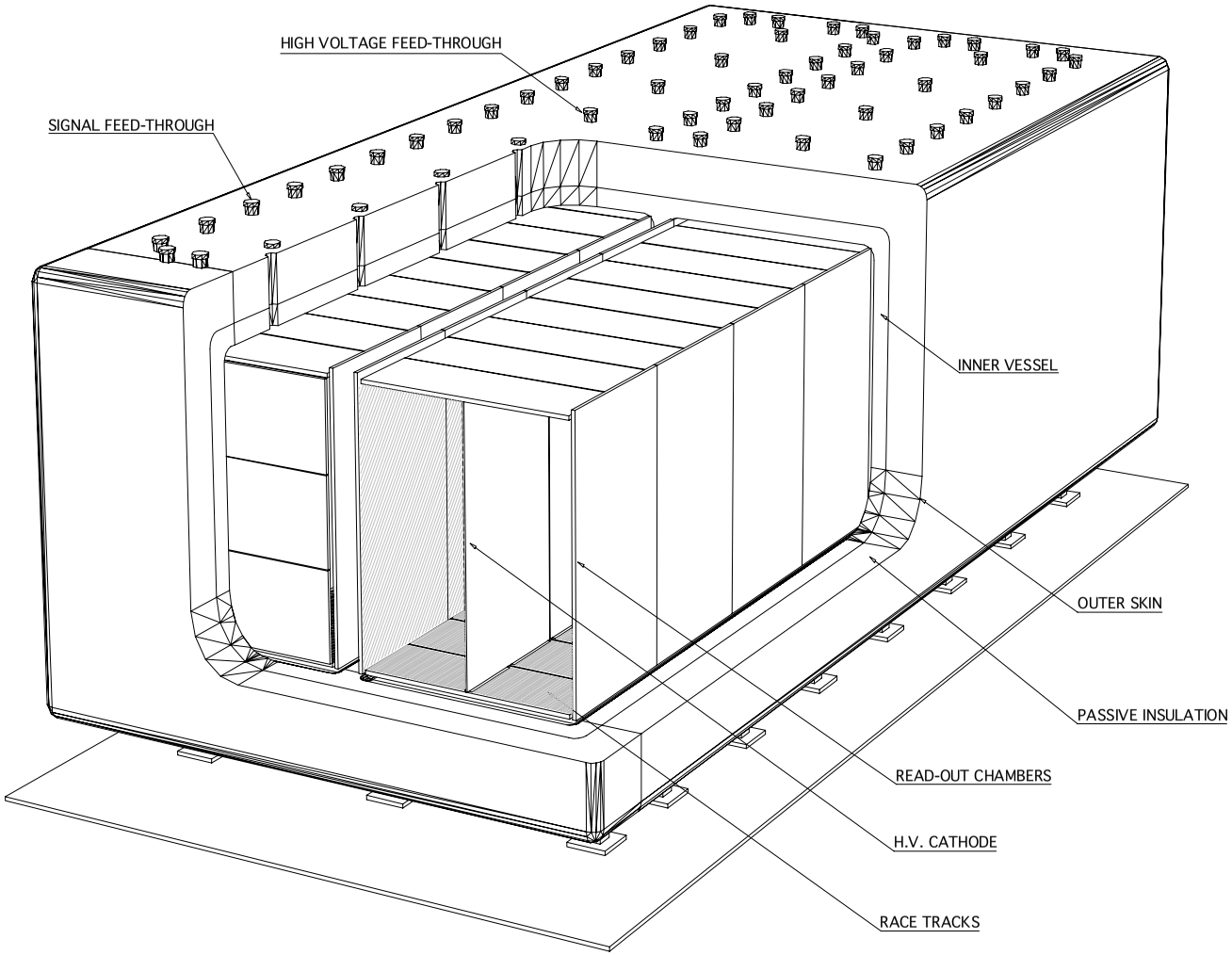

Figure 8: Icarus 600 ton

In the ICARUS 5000 ton proposal we presented two technical solutions for the read-out electrodes: the multilayer printed board and the wire chamber.

The first technique can be realized with two space-time orthogonal views only. This allows for a complete 3-D event reconstruction but without redundancy; this means that the detector could be blind along particular directions (e.g. the ones parallel to the printed strips).

The wire solution allows for multiple space-time views but it is more elaborate from the mechanical point of view and presents some weak points concerning safety and modularity.

Recently we have built a multilayer printed board on a medium scale (0.5x0.5 m^2). With it we tested the 3-D reconstruction capability of single tracks (cosmic muons) as a function of the polar and azimuthal angle. An example can be seen in Figure 9. The reconstruction efficiency is very close to one even for tracks whose direction is nearly parallel to that of the electric field in the drift region.

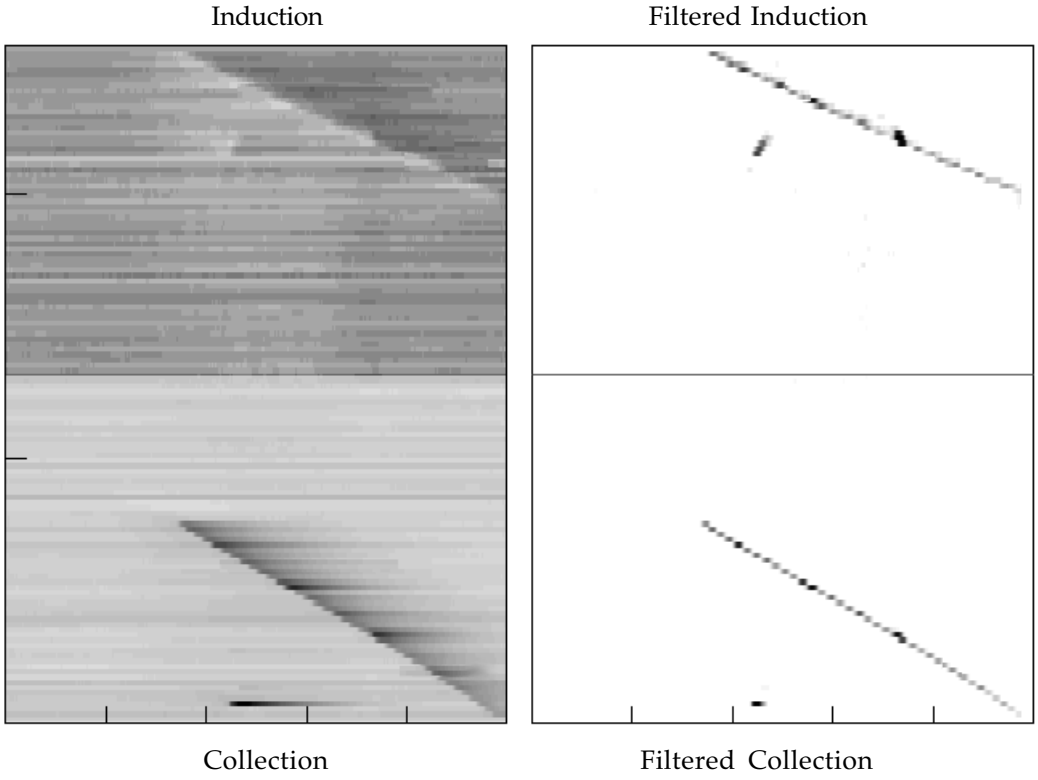

Figure 9: Two orthogonal space-time views of a cosmic muon as seen by the "multi-layer read-out chamber".

These very encouraging results lead us to believe that the definite solution will be a printed board equipped with a wire plane in front of it to add a third space-time view for redundancy. Figure 10 shows a possible layout for the 600 ton prototype with the wires stretched out vertically and the multilayer strips drawn at ± 45 ° with respect to the vertical direction. This read-out structure will be tested on a medium scale very soon to optimize the construction parameters.

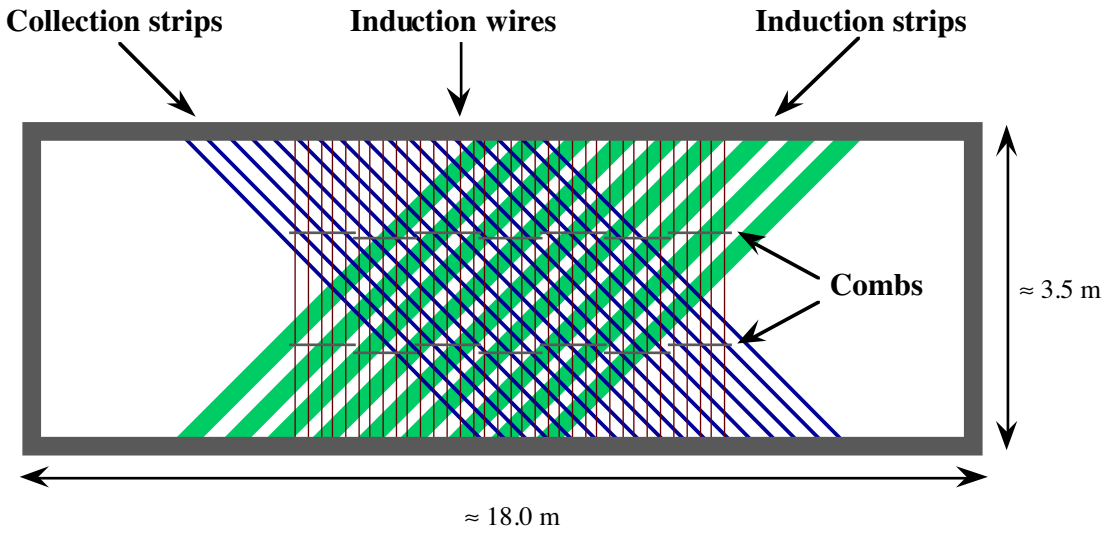

Figure 10: Schematic layout of the "multi-layer + wires" read-out chamber.

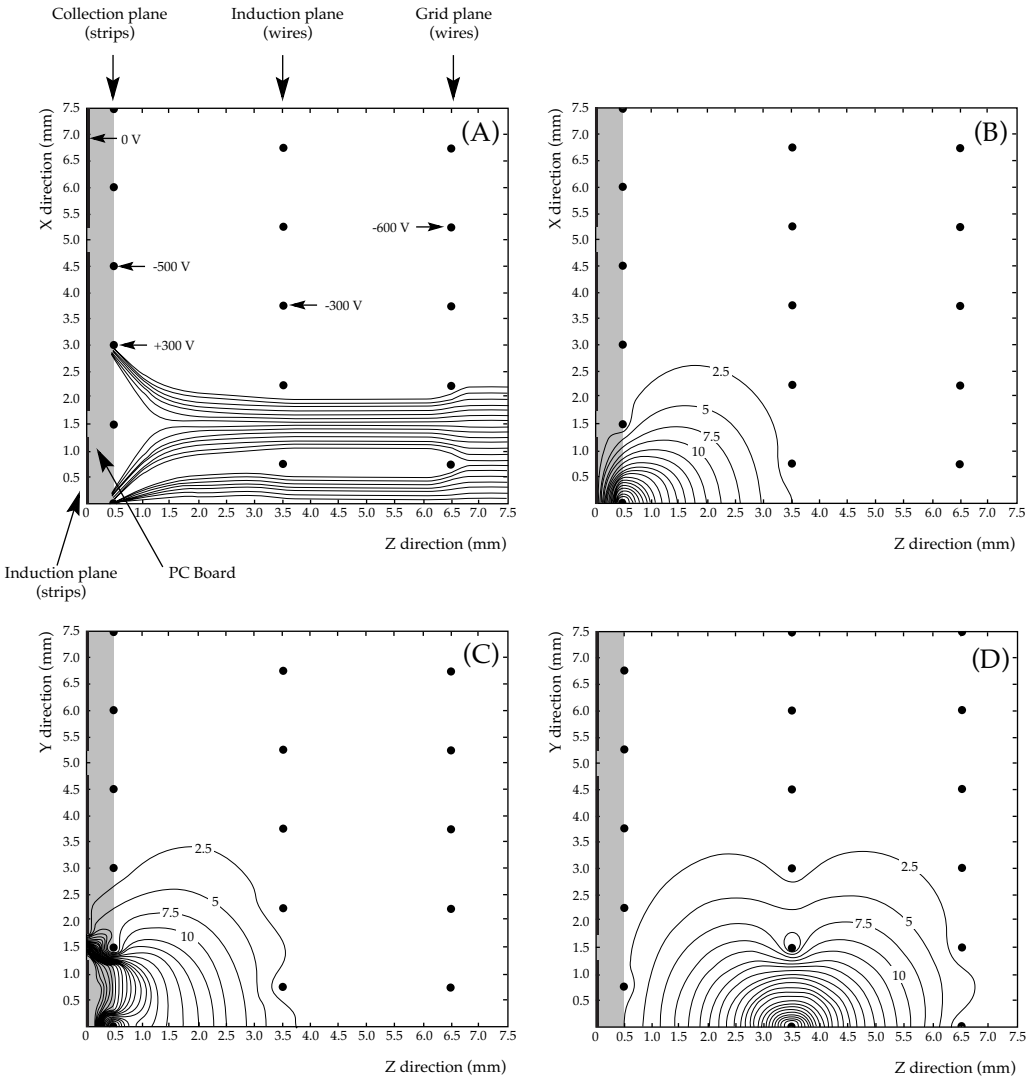

Figure 11: Electron drift lines in the "multilayer + wires" read-out chamber (A). Equi-induction map for collection strips (B), induction strips (C), induction wires (D).

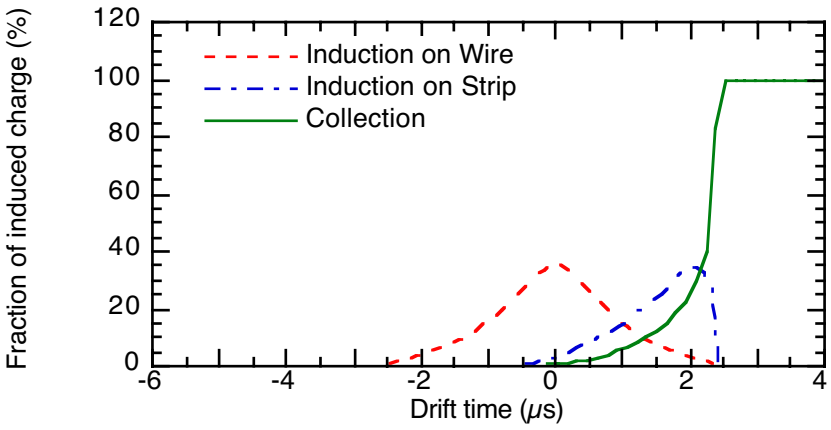

Figure 12: Basic charge signal shapes on the three different read-out electrodes.

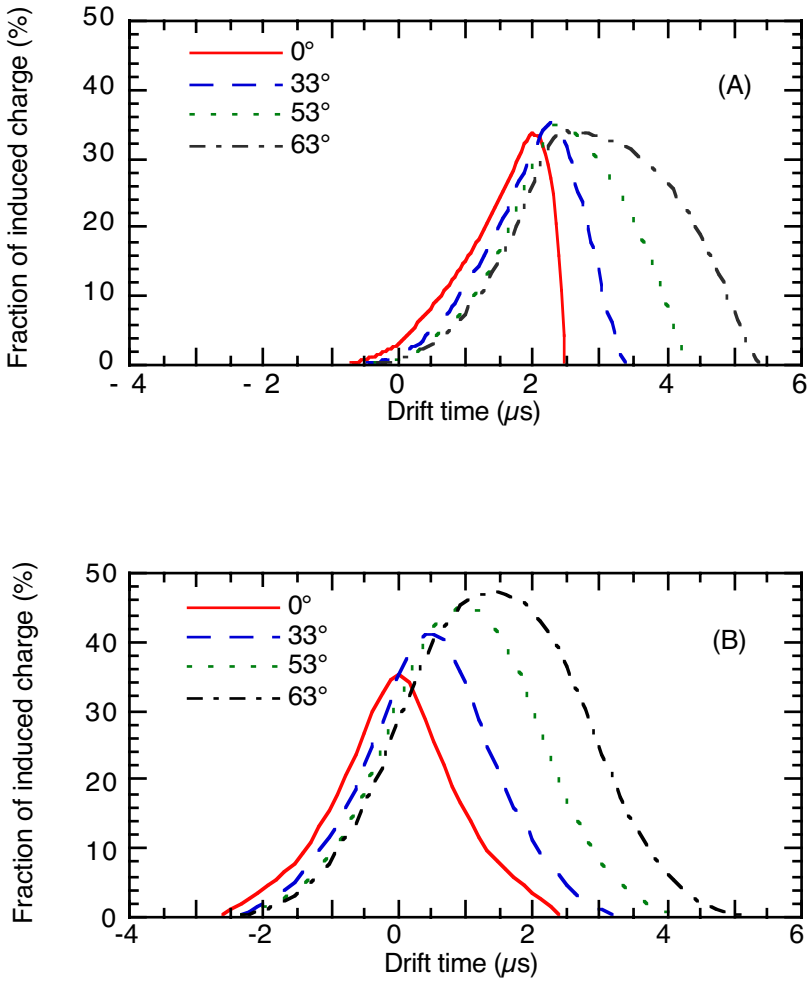

Figure 13: Charge induction signal shapes on induction strips (A) and wires (B) as a function of the track dip angle.

At present we rely on the results of electrostatic calculation to get the electric field drift lines and the induction signal shapes on the various electrodes. The comparison between simulation and real signals, made on our previous read-out structure, have proved that these calculations are sufficiently reliable to define to good approximation the electrode configuration for the test. A fine tuning will be performed after the analysis of the real data.

In order to prove that the "printed board plus wires" technique is realisable, in Figure 11a we show the field map with the electron trajectories ending on the collection strips. In Figures 11b,c,d the equi-induction maps for the three different read-out electrodes are reported; with them we have constructed the basic induction signals presented in Figure 12. Finally the signal shapes for the induction strips and induction wires are shown in Figure 13a,b as a function of the dip angle. The calculations have been performed for a pitch of 3 mm.

5.1 Three-dimensional read-out, field-shaping electrodes and cathodes.

The inner volume of an half-vessel is divided into two parts, giving a maximum drift length of the electrons equal to 1.64 m (Figure 14).

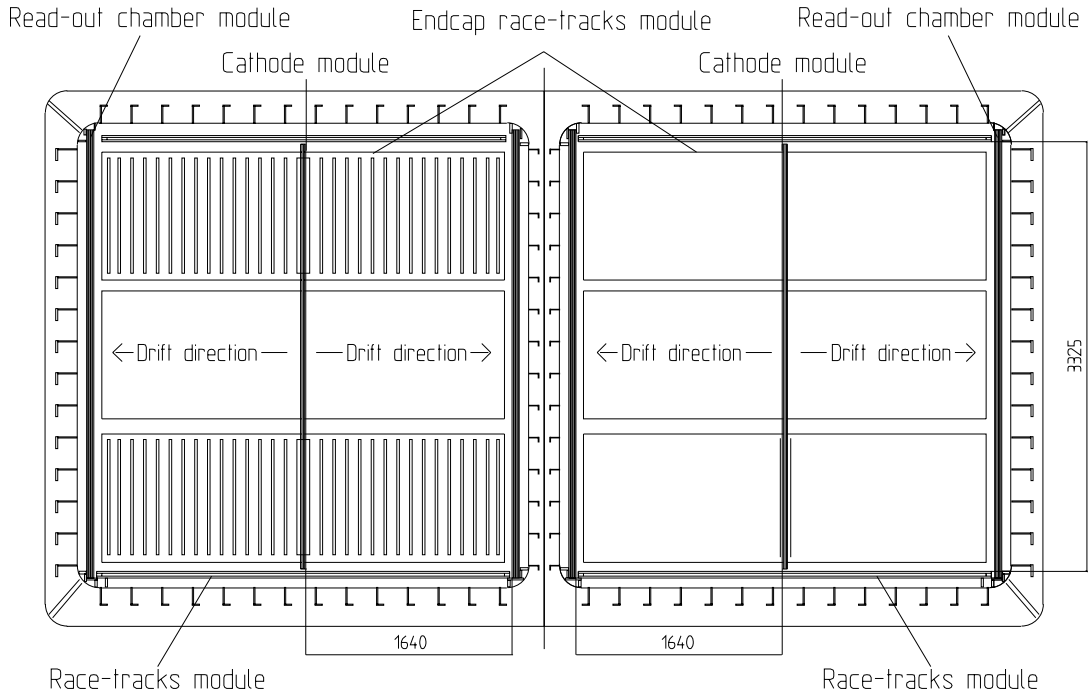

Figure 14: Transversal view of ICARUS 600t module.

The single-sided read-out chambers are positioned close to the vertical skins of the vessel, while the cathode is in the middle.

All the components of the detector will be built of modular elements, taking special care in minimising the number of in-plane electrical connections to form a "read-out strip" (maximum length ≈5.00 m). Therefore we will maximise both the module dimensions and the printed circuit length (see next

paragraph). At present, we have successfully produced very large printed circuits corresponding to the maximum substrate dimensions (≈4000x1100 mm^2) with similar geometry to the one we propose. This gives us more confidence on the quality of definition of the strips and on the reliability of this electrodes configuration.

5.1.1 Design and construction of the read-out chambers.

The ICARUS detector is foreseen to be equipped with four single read-out chambers whose dimensions are 3500x17900 mm^2. Each chamber is composed of eight modules; the dimensions are mainly determined by the size of the equipment used to build up the panels, by the modularity chosen for the electronic layout and the disposition of the printed sheets to avoid electrical connections within the single panel. At present this size is 3500x2240x56 mm^3 (Figure 15).

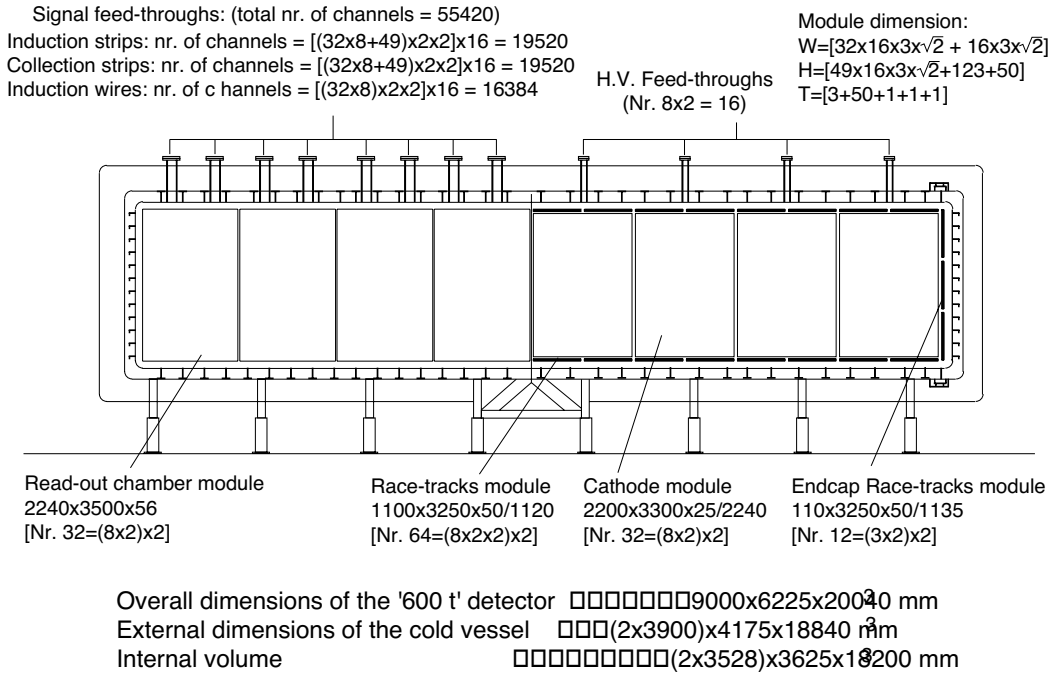

Figure 15: Longitudinal view of ICARUS 600 t module.

The read-out chamber module is defined as a panel supporting one multi-layer printed board (MLPB) plus two planes of wires (Figure 16).

The general considerations for the choice of the type of structure to realise the panel and the choice of the substrate materials are reported in the second volume of the "ICARUS 5000 t" proposal.

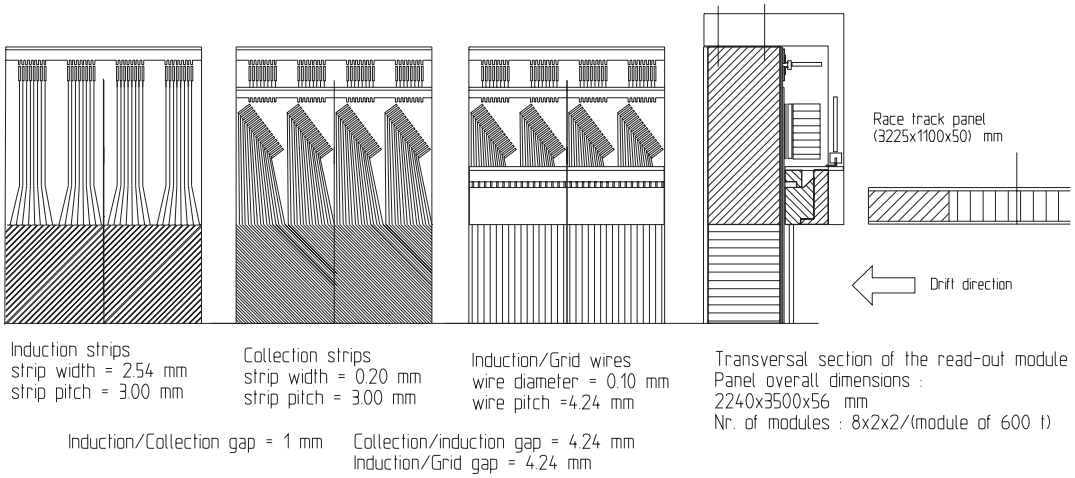

Figure 16: Simplified view of the superposed layers.

The mechanical structure of a typical read-out panel (Figure 17) is realised as follows.

1) An external sealing frame obtained by means of profiles of Stesalyte or G10, glued together on the corners (dimensions: ≈3500x50x40 and 2240x50x40 mm^3). The shape is optimised to provide a large sealing surface and a large support for the constrainment of cables, mother boards, connections, etc. Intermediate profiles will be inserted to reinforce the frame that must also withstand the wires load (Stesalyte or G10 ≈3420x50x30 mm^3).

2) Honeycomb sheets (hexagonal cells made of glass fibre reinforced plastic NOMEX®, 2550x1050x50 mm^3).

3) Fibreglass foils to seal the honeycomb volume (thickness ≈2x1.5mm). The metallised external face will provide a ground screening to the read-out plane.

4) A multi-layer board realising the induction and collection strips :

a) the collection strip plane: a printed circuit on G10 substrate (4000x1100x1.0 mm^3); the strips are at an angle of + 45° respect to the cryostat vertical axis (Figure 10): width=180 μm, thickness=35 μm, pitch=3.00 mm;

b) a glueing film;

c) the induction strip plane: a printed circuit on G10 substrate (4000x1100x1.0 mm^3); the strips are inclined of an angle of -45° with respect to the cryostat vertical : width=2.54 mm, thickness=35 μm, pitch=3.00 mm;

d) a glueing film;

e) a fibreglass foil to seal the honeycomb volume (thickness=1.0 mm).

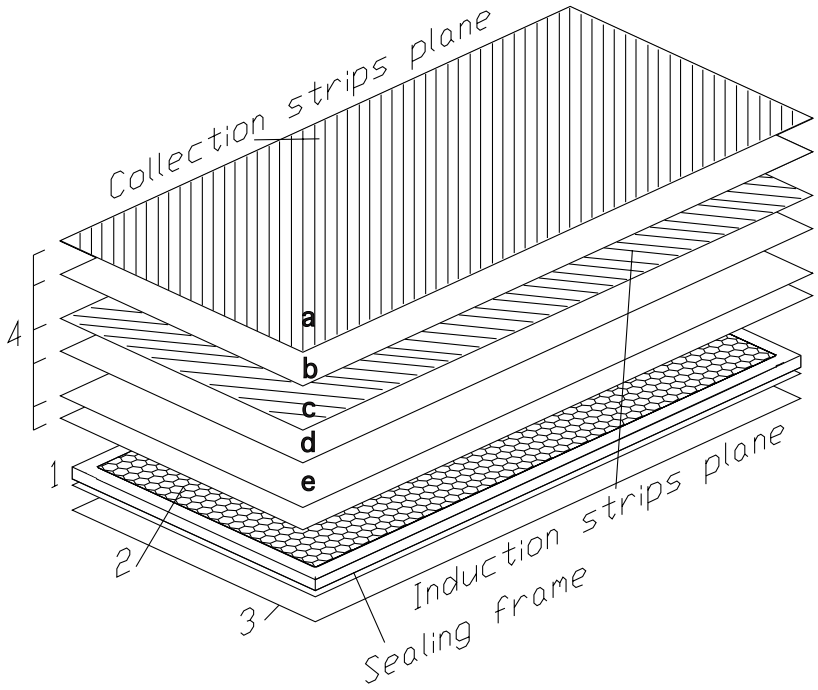

Figure 17: Exploded view of the read-out panel.

There are no electrical connections within a single module, to form a "read-out strip", as these are foreseen only between close modules, to allow a more easy check and repair, where needed.

We are also studying different solutions to completely avoid the connections to form a read-out channel.

The sandwich panels are all made with reference to an external frame, to maintain the correct positioning of all the substrates and to guarantee the uniformity of the general dimensions of the modules.

The two wire planes (Figure 10), realised by means of independent supports (pitch=3√2 mm, length=3.5m, nr. of supports/module= 32), are positioned vertically in front of the collection strips; the first being at a distance of 3√2 mm (induction), and the second at a distance of 2x(3√2) mm (grid). Each support holds 2x32 stainless steel wires of 0,1 mm of diameter.

The correct positioning of the wires along the length is obtained by means of drilled ceramic plates or combs (general dimensions : width=135 mm, heigth=12.7 mm, th=1.6 mm, holes diameter=0.15 mm), in number of two (three) x module, directly supported over the printed board plane.

5.2 High Voltage System.

Each half of the ICARUS-600 t detector (Figure 15) is electrically subdivided in 8 units. Each unit is made of :

- 1 central vertical cathode plane;
- 2 read-out chambers;

- 2 horizontal field shaping planes (*race tracks*) placed over and under the cathode plane.

The racetracks are used to keep uniform the electric field in the drift volume. The HV is supplied to the cathode of each unit via an individual feed-through placed in correspondence of the gap between the race track panels. Each race track plane is built by two panels.

The uniformity of the field at the detector endcaps is guaranteed by two extra vertical race track planes, segmented into 3 panels.

For additional details about the race-tracks system, refer to the corresponding section of our technical proposal [1].

6. Electronics

The read-out electronics for the liquid argon image chamber has already been extensively studied and tested in our 3 ton prototype. The system that will be used for the 600 ton module is based on these developments and is described in electronics section of our technical proposal [1].

References

[1] The ICARUS Collaboration, *"ICARUS II, a second-generation proton decay experiment and neutrino observatory at the Gran Sasso Laboratory"*, LNGS - 94/99 Vol. I & II, Proposal.